Macromolecular Bioscience

Macromolecular Bioscience
www.mbs-journal.de

RESEARCH ARTICLE

Exploring the Role of Cartilage Hypertrophy in Osteoarthritis Progression: A Structural and Biochemical Analysis of Glycosaminoglycan Loss and ECM Integrity

Chandrashish Roy[1] | Arti Sharma[2] | Juhi Chakraborty[1] | Soumik Siddhanta[2] | Sourabh Ghosh[1]

[1]Regenerative Engineering Laboratory, Department of Textile and Fiber Engineering, Indian Institute of Technology, New Delhi, India | [2]Department of Chemistry, Indian Institute of Technology, New Delhi, India

Correspondence: Sourabh Ghosh (sourabh.ghosh@textile.iitd.ac.in)

Received: 20 August 2025 | **Revised:** 17 November 2025 | **Accepted:** 1 December 2025

Keywords: attenuated total reflectance-fourier transform infrared spectroscopy (ATR-FTIR) | dimethyl methylene blue (DMMB) assay | extracellular matrix (ECM) | glycosaminoglycans (GAGs) | osteoarthritis (OA) | X-ray photoelectron spectroscopy (XPS)

ABSTRACT

It is a matter of debate whether chondrocytse hypertrophy is an active driver of age-related Osteoarthritis (OA) or a passive consequence of OA. Understanding the progression of hypertrophy can be crucial in developing effective disease-modifying therapeutics. To clarify this, we investigated biochemical signatures associated with human healthy cartilage and hypertrophic reactivation in human OA cartilage using a multimodal spectroscopic approach. Healthy adult cartilage and OA samples spanning different disease stages were analyzed using ATR-FTIR, XPS, Raman spectroscopy, DMMB and hydroxyproline assays, along with histology. Across all modalities, OA cartilage exhibited distinct molecular features consistent with a hypertrophic-like shift: pronounced GAG depletion, collagen network disruption, loss of collagen-specific spectral peaks, and elevated oxidative modifications in the ECM. Quantitative assays confirmed reduced GAG and total collagen content, aligning with biochemical patterns observed during endochondral maturation. Raman profiles further captured molecular rearrangements linked to matrix mineralization pathways typically associated with hypertrophic differentiation. Histological evaluation validated the progressive ECM disorganization and GAG loss, reinforcing the spectroscopic findings. Overall, these integrated results suggest that in OA, chondrocyte hypertrophy is not merely a passive consequence, but OA reflects a modified reactivation of endochondral ossification.

1 | Introduction

Osteoarthritis (OA) is the most prevalent kind of arthritis, impacting approximately 500 million individuals worldwide and posing considerable socioeconomic and health issues [1]. OA can be defined as a persistent and gradual age-related process of cartilage deterioration and joint remodeling. Second, there is a large variation in patient-specific clinical symptoms, as a vast processes lead to associated pain in whole joints, reduced mobility, joint dysfunction and other symptoms [1]. OA commonly affects weight-bearing joints such as the knees, hips, and spine, as well as smaller joints like those in the hands [2, 3]. The pathophysiology of the illness is multifaceted, involving biomechanical, metabolic, genetic, and inflammatory factors [4]. Further to this aging process, there might be other factors, like obesity, joint injury, joint loading and sustained mechanical stress, which further progress OA [5]. With the aging process, various structural and distinctive ECM modulations occur, which predominantly change in water, proteoglycans, glycosaminoglycans (GAGs), collagen, and several non-collagenous proteins [6]. Hydrophilic polysaccharides, including chondroitin sulphate and keratan sulphate, are conjugated to core proteins, creating

substantial proteoglycan aggregates that engage with hyaluronic acid [7]. Along with ECM degradation, there is vascularization (upregulated VEGF) and calcification (collagen type X, MMP9, MMP13) [8]. This process generates a new debate whether there is a connection between OA and the endochondral ossification process, i.e. OA is an inevitable "biological program", which is beneficial in the early stage of life (bone formation during young age), but harmful in the late stage of life [9]. The phenotypic transition of articular chondrocytes toward a hypertrophic state closely mirrors the molecular and cellular events of endochondral ossification, including the upregulation of type X collagen (COL10A1), runt-related transcription factor 2 (RUNX2), vascular endothelial growth factor (VEGF), and matrix metalloproteinases such as MMP-13. These changes collectively lead to extracellular matrix (ECM) degradation through enzymatic cleavage of collagen type II and aggrecan, pathological calcification of cartilage, and neo-angiogenesis at the osteochondral interface, processes that are aberrant in mature articular cartilage and contribute to irreversible structural deterioration and progression of OA

When cartilage is damaged, a number of courses can prevent it from regeneration, which starts as a chain of events that leads to degenerative disease states like OA [10]. This poses a major challenge in identifying solutions. From a molecular, biological, and mechanical perspective, cartilage reacts differently to injury and renewal in acute and chronic settings [11]. Acute cartilage injuries do, in fact, cause inflammation and immune cell activation, but if treatment is not received, these reactions can become detrimental and progress into a chronic pathological condition like OA [12]. In order to replace the damaged tissue and provide long-term symptomatic relief from OA manifestation, the researchers shifted their focus toward tissue engineering-based techniques to create phenotypically stable articular cartilage constructs. In order to achieve this, hydrogels have been explored widely owing to their biocompatibility and tunable mechanical characteristics, as they are ideal for regenerative applications such as bone and cartilage repair [13, 14]. For instance, silk fibroin-gelatin (SF-G), which intrinsically regulates Wnt/β-catenin signalling cascade, was explored to generate phenotypically stable articular cartilage via 3D bioprinting [15]. At higher cell density, the expression of articular cartilage markers, i.e. autotaxin (ATX), aggrecan (ACAN), and lubricin (PRG4), escalated remarkably. Even though the expression of articular cartilage markers was higher in 3D aggregates than the 3D bioprinted ones, however this was also accompanied by the expression of hypertrophic markers namely Indian hedgehog (IHH) and collagen X. Notably, the 3D bioprinted construct loaded with TVA-BMSCs suppressed hypertrophy and showed articular cartilage-specific gene expression, as seen by the minimal expression of collagen X, which is in accordance with our previously reported study [16]. Developing articular cartilage for load-bearing capabilities is hampered primarily by tissue engineers' inability to distinguish between artificial cartilage substitutes and the propensity of progenitor cells to either differentiate into articular or transient cartilage. Further, a poor knowledge of the cartilage tissue development at the embryonic level is one of the major reasons for its failure. Endochondral ossification, the major cause of OA progression, is brought about by certain signalling cascades, amely the Bone Morphogenetic Proteins (BMPs), Transforming Growth Factor beta (TGFβ), and Interleukin-1 (IL-1) that are essential for the development and remodeling of bones, frequently interacting and influencing one another. In order to evade the OA progression, Majumder et al. [17]. covalently coupled small molecules such as a bone morphogenetic protein (BMP) inhibitor, Low-dose naltrexone (LDN193189), TGFβ3, and IL1 receptor antagonist (IL1Ra) to SF-G bioink that were capable of tailoring the hypertrophic pathways and reversed the progression of OA, even under OA inducing conditions. Therefore, we presume that understanding the mechanisms involved in hypertrophic differentiation of chondrocytes at the cellular/molecular level can help develop appropriate OA models that can be helpful in the screening of anti-OA drugs. Many studies have been conducted to identify the molecular signs and related regulators of hypertrophy, but the fundamental mechanism and aetiology of the condition are still unknown. By maintaining the structure and hydration of the ECM, GAGs enable cartilage to endure everyday mechanical stress and fulfil its function in facilitating smooth joint articulation [18]. Surprisingly, in OA, the equilibrium between ECM formation and breakdown is disrupted, which in turn impacts GAG concentration [19]. With disease progression, there is a significant decline in GAG content, particularly chondroitin sulphate and keratan sulphate, resulting from enhanced breakdown and decreased production by chondrocytes [20]. The resultant depletion of GAGs markedly diminishes the cartilage's capacity for water retention, resulting in dehydration and impairing its ability to endure compressive stresses [21]. As a result, cartilage becomes increasingly vulnerable to injury, even under normal joint stress. This dehydration also impairs the interface between GAGs and the collagen network, compromising the structural integrity of the ECM. Insufficient GAG content compromises tissue resilience, leading to increased mechanical degradation of cartilage [22, 23], a hallmark of early-stage OA. In human patients with OA, the relationship between collagen degradation and proteoglycan loss in articular cartilage is yet unknown. Despite the characterization of tissue remodeling events at the articular cartilage, more nanoscale investigations would be highly instructive. To investigate macromolecular assemblies in the ECM and determine their destiny during OA, tissue characterisation at this level is, in fact, a pertinent method. Moreover, identifying the spectral changes in cartilage for the diagnosis of OA remains ambiguous.

Therefore, the aim of the present study is to identify the structural and molecular alterations in human cartilage ECM that take place during OA progression (Figure 1). We employed X-ray photoelectron spectroscopy (XPS), a surface science method that has seldom being applied to cartilage characterisation before. Further, we explored the potential of other advanced spectroscopic methods, such as ATR-FTIR, Raman spectroscopy, that provides useful insights for comprehending alterations in GAG and collagen concentration in OA samples compared with the control [21]. Biochemical estimation using DMMB assay and hydroxyproline assay was used to obtain knowledge at the protein level, especially in relation to the ECM. To the best of our knowledge this is the first study where a number of advanced spectroscopic methods have been used to determine the changes at the cellular/molecular level during OA progression. We strongly believe that these findings can provide a foundation for targeted therapeutic strategies aimed at preserving GAG and collagen, thus maintaining cartilage integrity and preventing OA progression.

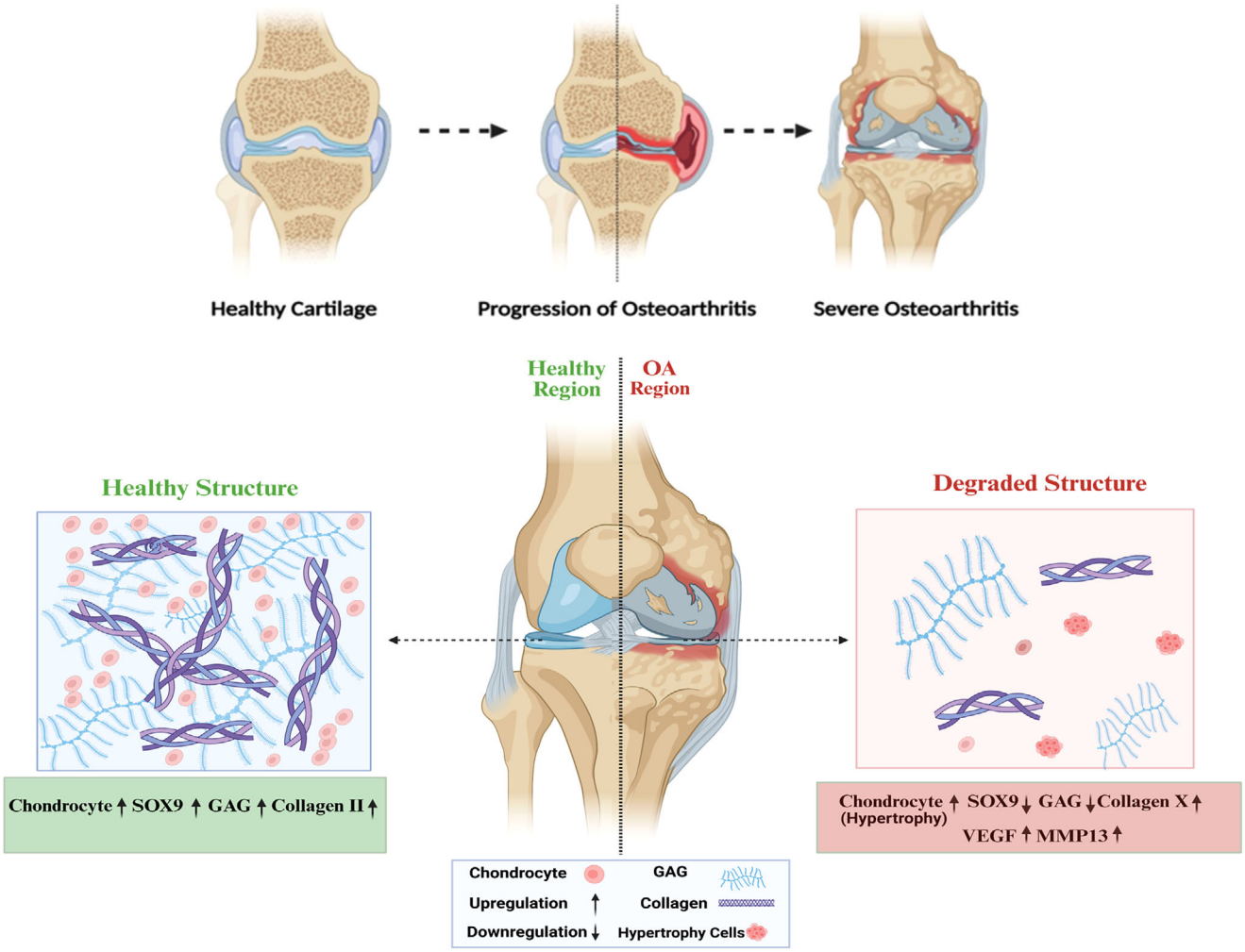

FIGURE 1 | Schematic illustration of healthy and osteoarthritic cartilage, highlighting structural differences in degraded cartilage regions during osteoarthritis progression. Hence, can the depletion of GAGs, along with the upregulation of MMP13 and collagen type X and the change in the ECM, suggest that OA involves a modified reactivation of endochondral ossification?.

2 | Materials and Methods

2.1 | Sample Collection and Clinical Classification

Cartilage samples were collected from four patients undergoing total knee replacement surgery at Indraprastha Apollo Hospital, New Delhi, India (ethical approval number-IAH-BMR-018/10-19). Healthy cartilage was obtained from two patients with no clinical or radiological evidence of OA, who underwent surgery for unrelated conditions, such as trauma and some mechanical complications. For the OA group, two patients diagnosed with OA were selected and classified using the Kellgren–Lawrence (K–L) grading system, which ranks OA severity based on radiographic criteria [24]. One patient was with Grade 2 OA, characterized by small osteophytes and mild joint space narrowing indicative of early degenerative changes, and one with Grade 3 OA, reflecting moderate joint space narrowing, pronounced osteophyte formation, and subchondral sclerosis [25]. Informed consent was secured from each participant (Table 1).

Upon excision, each cartilage sample was instantly frozen in liquid nitrogen to immediately preserve the biochemical and structural integrity of the ECM [26]. This rapid freezing technique effectively halts enzymatic activity, preventing the degradation of collagen, GAGs, and other critical ECM components, thus safeguarding the samples for subsequent analysis. Samples were stored at −80°C until further preparation [27]. Prior to spectroscopic and biochemical analyses, the cartilage samples underwent lyophilization, or freeze-drying, to remove water under low temperature and vacuum conditions, stabilizing the ECM structure and preventing degradation [28]. This process allowed for the optimal preservation of thermally sensitive ECM components, particularly collagen and GAGs. After lyophilization, the samples were subjected to cryogenic milling at −80°C, producing a fine, homogenous powder suitable for analysis. This powder form was critical for ensuring sample uniformity during spectroscopic measurements and enhancing data reliability. The samples were stored in desiccators at room temperature (RT) immediately prior to analysis in order to prevent moisture absorption during characterization [29]. The integrity and the concentration of GAG content in both healthy and OA cartilage were evaluated using a combination of spectroscopic techniques and biochemical assays to provide a detailed molecular profile [30].

TABLE 1 | Demographic and Clinical Details of Cartilage Samples Collected.

	Healthy Cartilage 1	Healthy Cartilage 2	Patient 1	Patient 2
Age	51	49	66	57
Grade	Normal	Normal	Grade 3	Grade 2
Date of Isolating	22-08-2024	22-08-2024	22-08-2024	22-08-2024

2.2 | Attenuated Total Reflectance-Fourier Transform Infrared Spectroscopy (ATR-FTIR)

To examine the molecular composition of ECM components non-destructively, ATR-FTIR spectroscopy was employed using a Nicolet iS10 ATR Spectrometer (Thermo Fisher Scientific). Approximately 2 mg of lyophilized cartilage sample was applied directly to the diamond crystal surface of the ATR unit, eliminating the need for extensive sample preparation while ensuring strong sample contact for high-quality spectral data. The spectral acquisition was performed over a wavenumber range of 4000–400 cm^{-1} at a resolution of 4 cm^{-1}, with 74 scans averaged per sample to optimize the signal-to-noise ratio and the samples were subsequently deconvoluted using Origin Pro 2023b (Origin Lab Corporation, Northampton, MA, USA). Prior to deconvolution, baseline correction and area normalization were performed [31]. This setup allowed for precise monitoring of molecular vibrations associated with ECM components, particularly collagen and GAGs [32].

2.3 | X-ray Photoelectron Spectroscopy (XPS)

XPS was used to analyse the elemental composition of cartilage surfaces, focusing on carbon, nitrogen, and oxygen as primary ECM elements in collagen and GAGs [33]. The lyophilized cartilage sample was pressed into thin films and mounted on a conductive substrate, then subjected to argon ion sputtering to clean the surface of contaminants [34]. Spectral acquisition utilized a PHI 5000 VersaProbe II XPS system, with high-resolution scans targeting the carbon (C 1s), nitrogen (N 1s), and oxygen (O 1s) peaks. These were measured at a pass energy of 23.5 eV and a resolution of 0.1 eV to determine the chemical states and concentrations of each element and were subsequently deconvoluted using OriginPro 2023b (Origin Lab Corporation, Northampton, MA, USA). Before deconvolution, baseline correction and area normalization were performed [35].

2.4 | Raman Spectroscopy

Complementing the ATR and XPS data, Raman spectroscopy provided additional insights into the vibrational modes of ECM molecular bonds [36]. The lyophilized cartilage samples were carefully placed on an aluminium slide, and spectra were recorded using an Olympus Horiba Xplora BX41 spectrometer with ~1 cm^{-1} resolution. A 785 nm laser with 10 mW power at the sample was used to minimize the interference of fluorescence from the biological samples. A 50X infinity corrected objective with NA 0.50 and 1200 grooves/mm grating was used for all the measurements [37]. Raman spectral acquisition spanned a wavenumber range of 1800–500 cm^{-1} region with exposure and acquisition time of 5 and 15 s, respectively, to increase the signal-to-noise ratio [38]. Further data processing, such as background subtraction and data smoothening, was done using adjacent averaging and the Savitzky–Golay method, respectively, in the origin 2020b software.

2.5 | Biochemical Estimation

2.5.1 | Dimethyl Methylene Blue (DMMB) Assay for GAG Quantification

The GAG content in cartilage samples was determined using the dimethyl methylene blue (DMMB) assay [39], a well-established method for detecting sulphated GAGs due to the binding affinity of DMMB dye to sulphate groups. Cartilage samples were collected from two patients, one with Grade 2 OA and another with Grade 3 OA, along with two healthy control samples. The cartilage was finely minced and subjected to enzymatic digestion with a papain solution (125 μg/mL), which had been prepared in 0.1 M sodium acetate buffer (pH 6.5) containing 5 mM L-cysteine and 5 mM EDTA [40]. The digestion process took place at 60°C for 24 h, effectively breaking down the cartilage matrix and releasing the GAGs from the ECM into the solution. After digestion, the samples were centrifuged at 10 000 x g for 10 min at RT to remove any remaining tissue debris, and the clear supernatant containing the released GAGs was carefully collected for further analysis.

The DMMB assay was prepared by dissolving 16 mg of DMMB in a 1 L solution containing 3.04 g glycine, 1.6 g NaCl, and 95 mL of 0.1 M acetic acid, adjusted to a pH of 3.5 using sodium formate. Chondroitin sulphate standards, ranging from 0 to 20 μg/mL, were prepared to generate a standard calibration curve for accurate GAG quantification. For each sample, 20 μL of the papain-digested cartilage extract or standard was pipetted into a 96-well microplate, followed by the addition of 200 μL of DMMB reagent [41]. The mixture was gently shaken for 5s to ensure homogeneous mixing. The absorbance of each well was measured immediately at 525 nm using a microplate reader to capture the metachromatic shift that occurs when the dye binds to sulphated GAGs. The GAG concentrations in the cartilage samples were calculated from the standard curve and compared across the OA and healthy control groups. Statistically significant reductions in GAG levels were observed in both Grade 2 and Grade 3 OA samples compared to the controls [42]. This decrease in GAG content reflected the degradation of the ECM and the loss of proteoglycans, particularly chondroitin sulphate and keratan sulphate, which are critical for the biomechanical properties of cartilage, including elasticity and load-bearing capacity. The lower GAG concentrations in OA cartilage were indicative of disease progression, as the depletion of proteoglycan indicates cartilage degeneration in the OA samples [43].

2.5.2 | Total Collagen Content

The total collagen content of the cartilage samples was determined by the hydroxyproline assay [44]. Proteinase K-treated samples underwent 18 h of hydrolysis in 12 M HCl at 120°C. The material was then dried for 48 h at 55°C under a chemical safety cabinet. The dried mass was reconstituted in H_2O. 100 µL of chloramine T/oxidation buffer mixture was added to each sample and standard, then incubated at RT for 20 min. 100 µL of the diluted dimethylaminobenzaldehyde reagent was added to each sample and standard, then incubated for 20 min at 60°C. The absorbance was measured at 560 nm. The readings were corrected by subtracting the blank value. The amount of hydroxyproline in the samples was determined based on the standard curve. The data were adjusted to reflect the dry weight of the cartilage samples before digestion. According to the reports, collagen contains 13% hydroxyproline or a ratio of 1:7.69 between hydroxyproline and collagen, based on which the estimation of the collagen content was carried out [44].

2.6 | Histological Processing of Cartilage Samples and Safranin-o-Staining

Cartilage samples were collected and classified into three groups: normal cartilage, Grade 2 OA, and Grade 3 OA, based on macroscopic and radiographic evaluation. Immediately after excision, the samples were fixed in 10% neutral-buffered formalin (NBF) for 48 h at RT to preserve tissue integrity and prevent enzymatic degradation. For samples containing subchondral bone, decalcification was carried out using 10% ethylenediaminetetraacetic acid (EDTA, pH 7.4) at 4°C for 2–4 weeks, with the solution being replaced every 48 h [45]. The decalcification process was monitored by assessing tissue pliability and radiographic imaging to ensure complete removal of mineralized components before further processing. Following fixation and decalcification, the tissues were subjected to graded ethanol dehydration (70%, 80%, 95%, and 100%), cleared in xylene, and embedded in paraffin. 5 µm-thick sections were obtained using a rotary microtome and mounted onto poly-L-lysine-coated glass slides to enhance tissue adherence. The sections were dried at 37°C overnight before proceeding with histological staining.

Histological assessment of GAG distribution was performed using safranin-o staining. Tissue sections were first deparaffinized in xylene (two changes, 5 min each) and rehydrated through a descending ethanol series (100%, 95%, 80%, and 70%), followed by a final rinse in distilled water. The sections were incubated in Weigert's Hematoxylin for 5 min to stain nuclei, followed by washing in running auto-claved water for 10 min to ensure differentiation of nuclear staining. To visualize collagen-rich structures, the sections were then stained with 0.02% Fast Green solution for 5 min, and excess dye was removed by briefly immersing the slides in 1% acetic acid for 2–3 s. Subsequently, the sections were counterstained with 0.1% safranin-o solution for 10 min, which selectively binds to negatively charged GAGs in the cartilage matrix [46]. After staining, the slides were sequentially dehydrated in graded ethanol (70%, 80%, 95%, and 100%), cleared in xylene, and mounted using DPX mounting medium for long-term preservation and analysis. Histological sections stained with Safranin O-Fast Green were examined using a Leica bright-field microscope at 10× and 40× magnifications to assess variations in GAG distribution, ECM integrity, and chondrocyte morphology across normal and OA cartilage samples. To ensure reproducibility, images were acquired under identical exposure conditions using a high-resolution digital camera system attached to the microscope.

2.7 | Immunohistochemical Detection of Collagen II and Collagen X

For immunohistochemical staining, paraffin-embedded sections from the previous step were deparaffinized in two changes of xylene (10 min each), followed by rehydration through a descending ethanol series (100%, 95%, and 70%) and a final rinse in distilled water. To enhance antigen accessibility within the dense cartilage ECM, enzymatic antigen retrieval was performed by incubating the sections in 0.05% hyaluronidase (Sigma–Aldrich, H3506) dissolved in PBS at 37°C for 30 min. Endogenous peroxidase activity was quenched by treating the sections with 3% hydrogen peroxide in PBS for 10 min at RT. To block nonspecific binding, slides were incubated with 5% bovine serum albumin (BSA) in PBS for 1 h at RT. Primary antibodies targeting human collagen II (Abcam, ab34712; dilution 1:200) and collagen X (Abcam, ab58632; dilution 1:200) were diluted in 1% BSA/PBS and applied to separate tissue sections. Incubation was performed overnight at 4°C in a humidified chamber to ensure strong and specific antigen–antibody binding. The following day, slides were rinsed thoroughly in PBS and incubated for 1 h at RT in the dark with a horseradish peroxidase (HRP)-conjugated goat anti-human IgG secondary antibody (Invitrogen, A18811; dilution 1:500). Immunoreactivity was visualized using a 3,3′-diaminobenzidine (DAB) substrate kit (Vector Laboratories, SK-4100), which produces a brown chromogenic signal at the site of antigen localization. The reaction was microscopically monitored and terminated uniformly across all samples to maintain consistent staining intensity. Slides were then rinsed in distilled water, dehydrated through an ascending ethanol gradient, cleared in xylene, and permanently mounted using DPX mounting medium. To enable specific visualization of extracellular collagen, nuclear counterstaining was intentionally omitted to avoid signal interference. General tissue structure and ECM organization were first assessed using brightfield mode on the Leica TCS SP8 confocal microscope. For collagen detection, sections were imaged using the confocal fluorescence mode. Fluorescent signals corresponding to collagen II and type X immunolabeling were acquired at an excitation wavelength of 552 nm. All images were captured at 5× and 20× magnification with fixed laser intensity, detector gain, and exposure time across all experimental groups to ensure consistency and comparability. This imaging strategy allowed high-resolution, section-specific analysis of collagen distribution in normal healthy cartilage, Grade 2 and Grade 3 OA samples.

2.8 | Quality Control and Reproducibility

All analyses were conducted using standardized and validated protocols to ensure reliability and reproducibility. Measurements for each technique were independently repeated, and consistent trends were observed across spectroscopic, biochemical, and histological datasets. Detailed parameters for sample preparation,

data acquisition, and spectral interpretation are provided to facilitate reproducibility. A multimodal comparison of GAG depletion across all the techniques, along with inter-method correlation was also conducted (Figure S1)

2.9 | Statistical Analysis

All experiments were conducted in triplicate to ensure the reliability and reproducibility of the data. The results were expressed as mean ± standard deviation. Statistical analysis was performed using GraphPad Prism 9.0 software. One-way analysis of variance (ANOVA) was conducted to compare the differences between healthy and osteoarthritic cartilage samples across various characterization methods. Post-hoc analysis was performed using Tukey's test to identify specific group differences. A p-value of 0.05 was considered statistically significant for all tests, indicating meaningful differences in ECM composition and degradation between the two groups.

All analyses were conducted using standardized and validated protocols to ensure reliability and reproducibility. Measurements for each technique were independently repeated, and consistent trends were observed across spectroscopic, biochemical, and histological datasets. Detailed parameters for sample preparation, data acquisition, and spectral interpretation are provided to facilitate reproducibility.

3 | Results

3.1 | XPS Analysis

XPS was utilized to investigate the surface-sensitive elemental and chemical composition of ECM components in both healthy and OA cartilage samples [47]. This study focused particularly on detecting variations in nitrogen, carbon, and oxygen content within the ECM, which consisted predominantly of collagen and GAGs [48]. Collagen contained a high concentration of nitrogen due to peptide bonds between amino acids, while GAGs incorporated nitrogen and oxygen through their carbohydrate-based structures. XPS analysis revealed a significant depletion in nitrogen content, which indicated a decline in GAG concentration, a key marker of OA progression. This depletion reflected the loss of GAGs and collagen, suggesting compromised structural and biochemical properties within the ECM that are critical for maintaining cartilage function.

3.1.1 | Comparative Analysis of Healthy and Grade 3 OA Cartilage in Patient 1

The XPS spectra of healthy cartilage illustrated distinct peaks for nitrogen (N 1s), carbon (C 1s), and oxygen (O 1s), which were closely tied to the high concentrations of GAGs and collagen that comprised the ECM of cartilage. The nitrogen peak, observed at approximately 399 eV, was noteworthy, as it indicated nitrogen-containing functional groups, such as amine (—NH_2) and amide (—$CONH_2$) groups (Figure 2A). These functional groups are integral components of both collagens, a protein rich in amide linkages, and GAGs, which contained nitrogenous sugar derivatives like N-acetylglucosamine.

In contrast, the XPS spectra for the Grade 3 OA cartilage sample from patient 1 (Figure 2B), revealed considerable alterations, particularly with respect to the nitrogen, carbon, and oxygen peaks, all of which were significantly reduced or absent. Surprisingly, no peak was observed at 399 eV.

3.1.2 | Comparative Analysis of Healthy and Grade 2 OA Cartilage in Patient 2

The XPS spectra for the healthy cartilage in patient 2 exhibited strong peaks, including a prominent nitrogen (N 1s) peak at a binding energy of approximately 399 eV (Figure 2C,D). This peak was indicative of substantial nitrogen-containing ECM components, specifically GAGs, and collagen, which are essential for maintaining cartilage structure and function. In contrast, the Grade 2 OA cartilage sample displayed a nitrogen peak at the same binding energy; however, its intensity was notably diminished compared to that of the healthy cartilage. In addition to the reduction in the nitrogen peak, the analysis revealed corresponding decreases in the carbon (C 1s) and oxygen (O 1s) peaks for the Grade 2 OA cartilage.

3.1.3 | Deconvolution of Carbon and Nitrogen Peaks

After obtaining the XPS spectra results indicating the presence of various functional groups, we further deconvoluted the carbon (C 1s) peaks to identify specific chemical functionalities within the healthy cartilage sample (Figure 3A,B). The deconvolution revealed three distinct peaks; each associated with a unique binding energy that corresponds to particular molecular groups in the ECM. The first peak, observed at 282.0 eV, was assigned to C—C/C—H bonds, which represent aliphatic hydrocarbons. These groups are structural components typically found in healthy cartilage and contribute to the tissue's resilience and mechanical stability [49]. The second peak, located at 283.3 eV, corresponded to C—O bonds, characteristic of alcohol or ether groups. This functional group is often associated with GAGs, molecules crucial for the structural and biomechanical properties of cartilage. The third peak, at 285.0 eV, indicated the presence of C—N bonds, which likely correspond to amine groups linked to proteins such as collagen and proteoglycans. The presence of these functional groups highlights the essential role of collagen, GAGs, and proteoglycans in maintaining the integrity and function of healthy cartilage tissue (Figure 3A,B) [49].

Further, the deconvolution analysis of carbon peaks for a Grade 3 OA cartilage sample, revealed significant differences when compared to healthy cartilage (Figure 4A,B). The C—C/C—H bonding group, which was identified in both healthy and OA cartilage, displayed a slightly lower binding energy in the OA sample at 281.0 eV. This shift suggests an altered carbon bonding environment, likely resulting from cartilage degradation. The presence of the C—O group at 282.5 eV in the OA sample indicated a minor shift from its position in healthy cartilage, suggesting structural changes within the molecular composition of the car-

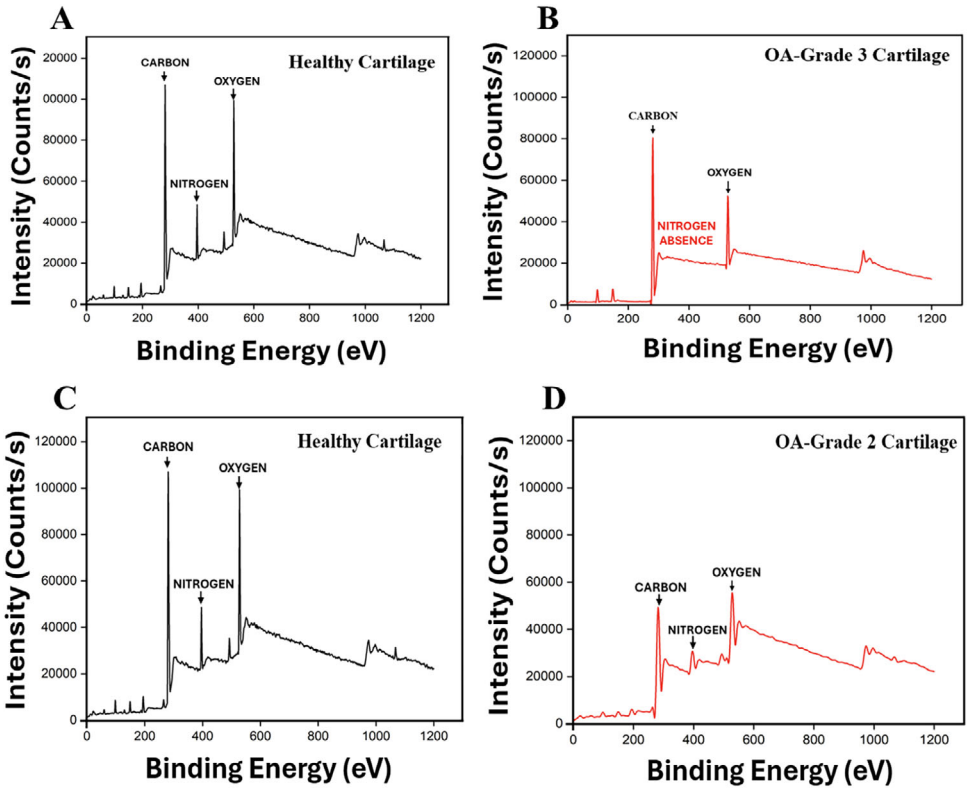

FIGURE 2 | XPS spectra of healthy and osteoarthritic cartilage. (A, C) Healthy cartilage samples show distinct peaks for carbon (~285 eV), oxygen (~532 eV), and nitrogen (~400 eV), indicating the presence of key ECM components such as collagen and GAGs. (B) Grade 3 OA cartilage exhibits peaks for carbon and oxygen but lacks the nitrogen peak (~400 eV), signifying significant degradation of nitrogen-containing ECM components. (D) Grade 2 OA cartilage shows reduced nitrogen intensity compared to healthy cartilage, indicating partial degradation of nitrogen-rich compounds during disease progression.

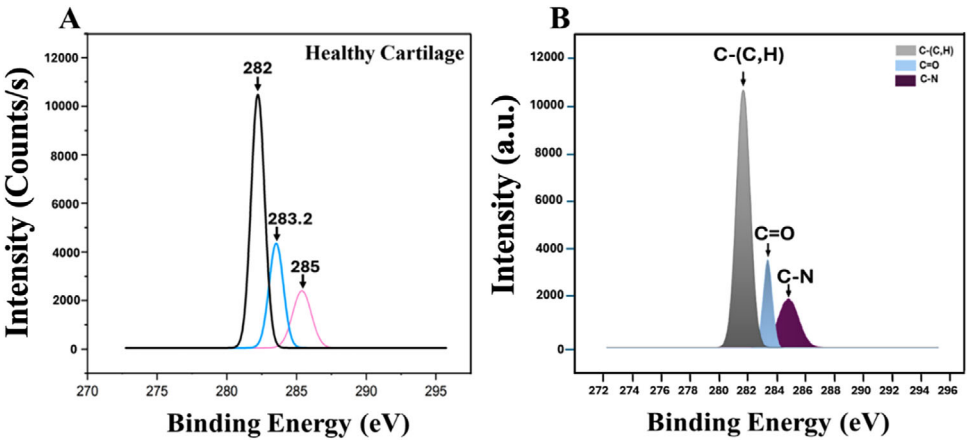

FIGURE 3 | Deconvoluted XPS C1s spectra for healthy cartilage. (A) shows binding energies of functional groups. (B) illustrates peaks corresponding to different carbon chemical states.

tilage matrix due to advanced OA changes [49, 50]. A particularly prominent finding was the absence of the C—N bonding group, which appeared at 285.0 eV in healthy cartilage but was missing in the Grade 3 OA sample. This absence is indicative of the depletion of nitrogen-containing biomolecules, such as collagen and GAGs, essential for cartilage integrity and function. The lack of these compounds aligns with the characteristic features of advanced OA, where cartilage degradation leads to a loss of structural components necessary for functional capacity. This depletion of the ECM components provides evidence of the extensive matrix breakdown that is commonly observed in Grade 3 OA cartilage. We also conducted a deconvolution for the carbon peaks for the Grade 2 OA sample, as illustrated in Figure 4C,D. The C—C/C—H group was observed at 281.0 eV, consistent with the findings from the Grade 3 sample. The C—O group was identified at 282.5 eV, aligning with the spectra of both the Grade

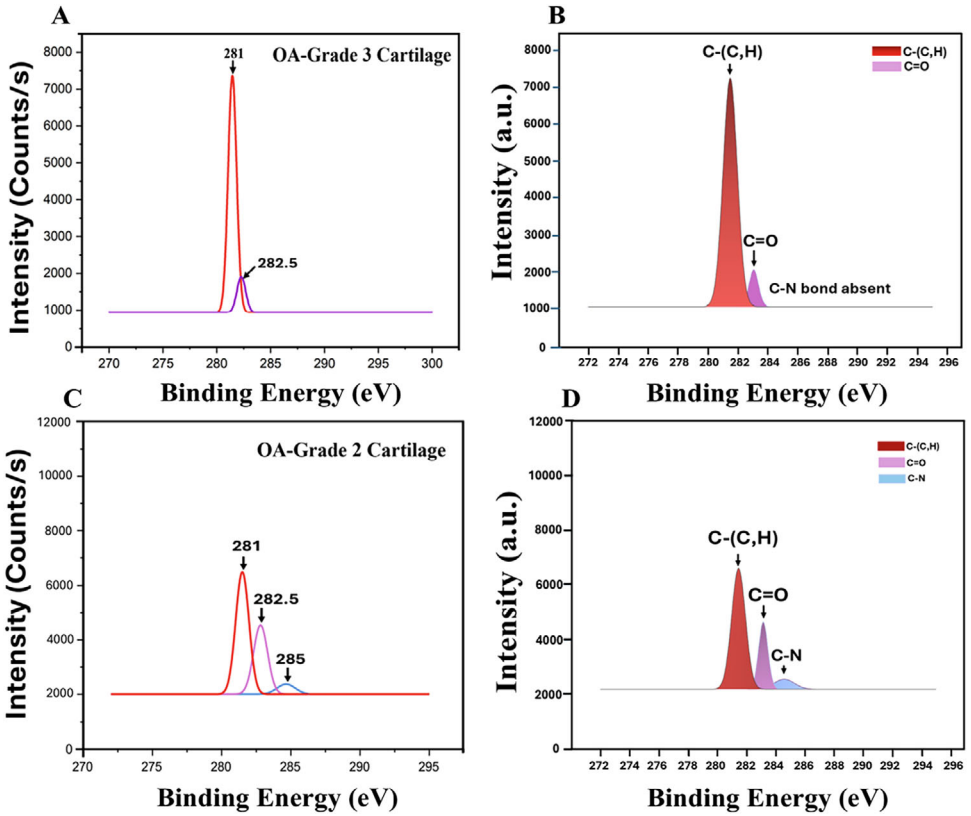

FIGURE 4 | XPS Carbon Spectra Deconvolution for Grade 2 and Grade 3 Osteoarthritis Cartilage Samples (A) Deconvoluted XPS spectrum for Grade 3 OA cartilage, showing binding energy peaks at 281 and 282.5 eV, corresponding to C— (C,H) and C═O bonds, respectively. (B) Illustration of the distinct carbon chemical states in Grade 3 OA cartilage, highlighting the absence of the C—N bond. (C) Deconvoluted XPS spectrum for Grade 2 OA cartilage, with binding energy peaks at 281, 282.5, and 285 eV, corresponding to C— (C, H), C═O, and C—N bonds, respectively. (D) Illustration of the distinct carbon chemical states in Grade 2 OA cartilage, confirming a low-intensity C—N bond compared to other bonds.

3 and healthy cartilage samples. Particularly, the C—N group was detected at 285.0 eV in the Grade 2 OA sample; however, its intensity was significantly lower than that observed in healthy cartilage. This result suggested that, while the degradation of collagen and GAGs had commenced, these components were not entirely absent in Grade 2 OA, in contrast to the findings in Grade 3 OA. The reduced intensity of the C—N peak in Grade 2 indicated a diminished yet detectable presence of GAGs and collagen, implying an intermediate state of cartilage degeneration in Grade 2 OA compared to the more advanced degeneration observed in Grade 3 OA [49].

To further investigate the compositional differences between healthy and OA cartilage, the nitrogen (N 1s) peaks were deconvoluted for all samples (Figure 5A,B). In the healthy cartilage sample, a prominent nitride peak was detected at 395.5 eV, corresponding to nitrogen-containing compounds such as collagen and proteoglycans. This strong nitrogen signal is a characteristic feature of healthy cartilage, where collagen and GAGs are present in substantial quantities, contributing to the structural and functional integrity of the cartilage matrix. In comparison, the Grade 3 OA sample showed a complete absence of the nitrogen peak (Figure 5B), indicating a marked depletion of nitrogenous compounds, including collagen and GAGs, in advanced OA. This absence of nitrogen in the OA sample is consistent with the previously observed lack of the C—N peak in the carbon spectrum, further reinforcing the conclusion that Grade 3 OA is associated with severe degradation of the ECM. These findings underscore the significant loss of essential biomolecules in advanced OA cartilage, contributing to its compromised structural and functional capacity. In the analysis of the Grade 2 OA sample, a nitride peak was detected at 395.7 eV, indicating that nitrogen-containing compounds, like GAGs and collagen, were still present in the cartilage. Although this nitrogen peak was relatively weak in Figure 5C,D, its presence suggested that GAGs, which are essential for the structural integrity and function of cartilage, were still detectable, but in lower amounts. In comparison, Grade 3 OA showed much more severe degradation, with nitrogen peaks largely absent due to the breakdown of nitrogen-rich biomolecules. The low-intensity nitrogen peak in Grade 2 OA indicated that the ECM was still partially preserved, particularly the GAGs.

3.2 | ATR-FTIR Spectroscopy

ATR-FTIR spectroscopy was employed to examine the molecular-level changes in functional groups related to collagen and GAGs within the ECM of cartilage [51]. This technique provides complementary information to XPS by detecting vibrational modes of chemical bonds, particularly focusing on amide groups (from collagen) and carbohydrate linkages (from GAGs).

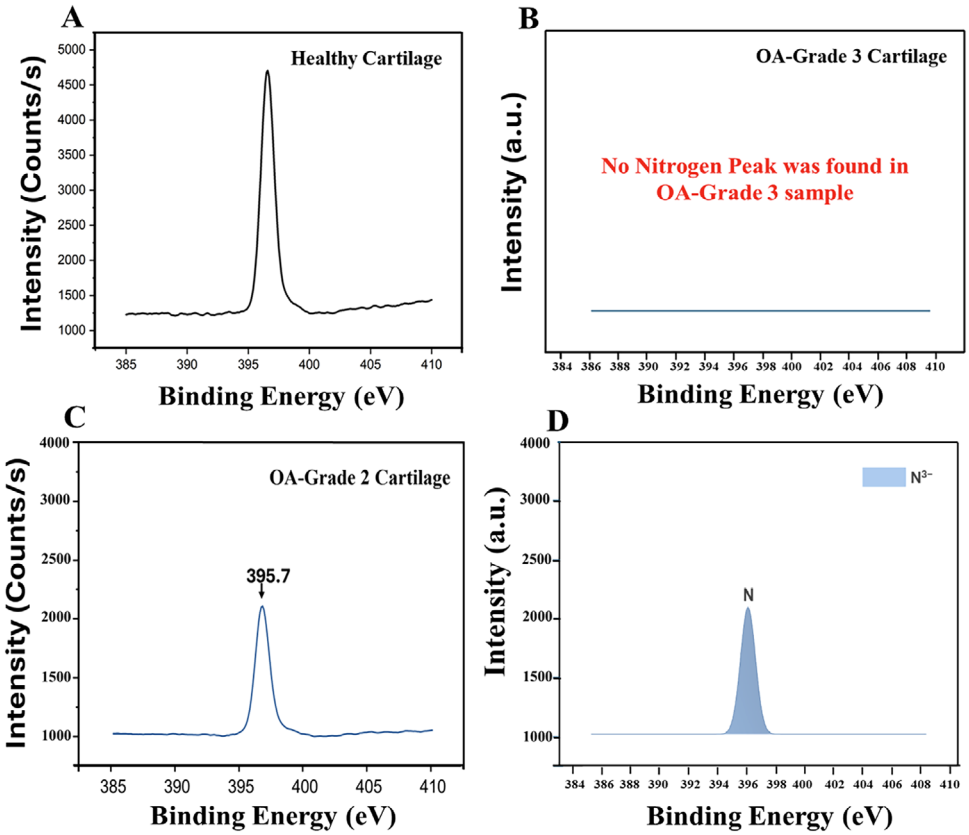

FIGURE 5 | Deconvolution of XPS nitrogen spectra across different cartilage samples with varying grades of osteoarthritis. (A) XPS nitrogen spectrum for healthy cartilage, displaying a distinct nitrogen peak at approximately 395.5 eV, indicative of nitrogen-containing components. (B) XPS nitrogen spectrum for cartilage from a Grade 3 OA patient, where no detectable nitrogen peak is observed, confirming the absence of nitrogen species such as N^{3-} in the sample. (C) XPS nitrogen spectrum for cartilage from a Grade 2 OA patient, showing the presence of a nitrogen peak (~395.7 eV) associated with nitrogen-containing compounds, albeit with lower intensity compared to healthy cartilage. (D) Deconvolution of the nitrogen peak (~395.7 eV) in the Grade 2 OA sample, confirming the presence of the N^{3-} component but at a reduced intensity compared to healthy cartilage.

3.2.1 | Comparative Analysis of Healthy and Grade 3 OA Cartilage

In healthy cartilage, strong characteristic absorption peaks were observed in the mid-infrared region, (Figure 6A) which corresponds to major ECM constituents. The amide II band at ~1537 cm^{-1} arises from N—H bending and C—N stretching of peptide bonds and is primarily attributed to collagen and proteoglycan structures. Its high intensity indicates a well-organized and densely cross-linked proteinaceous ECM, essential for maintaining the tensile strength and load-bearing properties of cartilage [52, 53]. A distinct C—O stretching band at ~1385 cm^{-1} was also detected, which corresponds to vibrational modes in the carbohydrate backbone of GAGs such as chondroitin sulphate and keratan sulphate. These polysaccharides are covalently attached to core proteins to form proteoglycans, contributing to the osmotic and compressive resilience of the ECM. Additionally, the peak at ~1337 cm^{-1}, assigned to collagen II, was clearly visible. This peak reflects the triple-helical conformation and side-chain vibrations specific to mature fibrillar collagen, the dominant collagen subtype in articular cartilage. The intact presence of collagen II supports ECM integrity and confirms the biochemical stability of healthy cartilage. In contrast, Grade 3 OA cartilage exhibited pronounced spectral changes. As shown in Figure 6A, there was a substantial reduction in the intensity of the amide II (1537 cm^{-1}) and C—O stretching (1385 cm^{-1}) bands, indicating degradation of both collagen and proteoglycans. The collagen II peak (1337 cm^{-1}) was significantly diminished, reflecting fragmentation and denaturation of the collagen fibrils. This spectral shift reflects the deterioration of the ECM scaffold, resulting in decreased tensile strength and increased susceptibility to mechanical damage [54]. Most notably, Figure 6C revealed the appearance of a unique and intense band at ~1041 cm^{-1}, attributed to collagen X, a well-established marker of hypertrophic chondrocytes. Unlike collagen II, which maintains the structural and functional integrity of articular cartilage, collagen X is typically expressed during endochondral ossification and in hypertrophic zones during pathological cartilage remodeling [55]. The emergence of this peak in Grade 3 OA reflects a phenotypic shift of chondrocytes toward hypertrophy, characterized by increased cell size, matrix mineralization, and upregulation of catabolic enzymes such as MMP-13 and ADAMTS-5. The presence of collagen X thus indicates the onset of terminal chondrocyte differentiation, where hypertrophic chondrocytes play a critical role in driving the progression of OA.

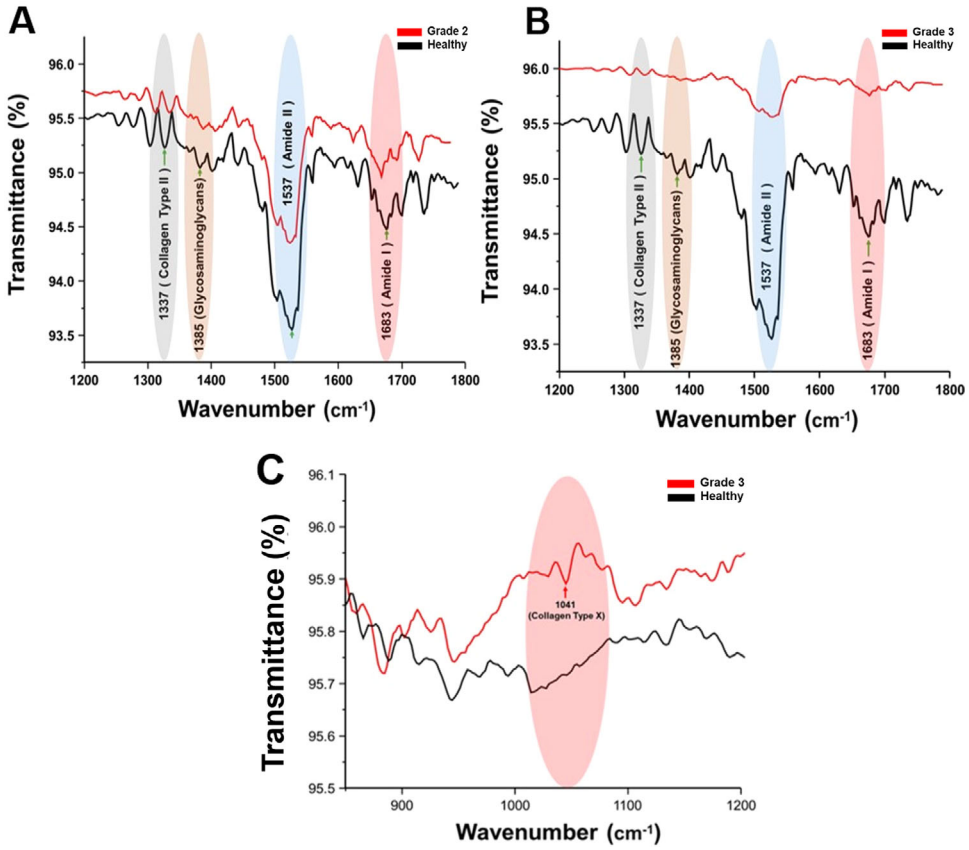

FIGURE 6 | ATR-FTIR spectral analysis of healthy and Osteoarthritic (OA) Cartilage. (A–C) ATR-FTIR spectra comparing healthy cartilage (black) with Grade 2 (Red) and Grade 3 OA cartilage (Red) from Patient 1. (A) Healthy cartilage shows distinct peaks at 1337 cm^{-1} (Collagen II), 1385 cm^{-1} (Glycosaminoglycans), and 1537 cm^{-1} (Amide II), which are diminished in Grade 3 OA, indicating collagen loss and ECM degradation.(B) Grade 2 OA cartilage displays moderate reductions in collagen II, GAGs, and Amide II bands, reflecting partial ECM deterioration. (C) Grade 3 OA cartilage shows a prominent new peak at 1041 cm^{-1}, corresponding to collagen X, indicating chondrocyte hypertrophy and pathological remodeling.

3.2.2 | Comparative Analysis of Healthy and Grade 2 OA Cartilage

In Grade 2 OA cartilage (Figure 6B), the amide II peak (~1537 cm^{-1}) was still evident but exhibited moderate reduction in intensity compared to the healthy cartilage. This suggests early onset of matrix degradation, with partial denaturation of collagen and reduced proteoglycan content. While the ECM scaffold is still present, its biochemical integrity is beginning to decline, leading to compromised mechanical stability. The C—O stretching band at ~1385 cm^{-1}, corresponding to GAGs, also displayed decreased intensity, indicating partial depletion of GAGs. Since GAGs are critical for maintaining tissue hydration, even this moderate loss can affect the cartilage's viscoelastic behavior and its ability to withstand compressive loading. The collagen II peak at 1337 cm^{-1} also exhibited a noticeable decrease in intensity, reflecting the initial degradation of the native fibrillar collagen network.

3.3 | Raman Spectroscopy

We explored Raman spectroscopy to investigate compositional changes in the ECM matrix of the cartilage samples from different patients. Raman spectroscopy, a vibrational spectroscopic technique akin to FTIR and near-infrared (NIR) spectroscopy, offers distinct advantages for biomedical analysis. It is inherently label-free, non-invasive, and requires minimal to no sample preparation while providing high spatial-resolution imaging capabilities [56]. Unlike ATR-FTIR, Raman spectroscopy is unaffected by water interference, rendering it particularly suitable for monitoring molecular and biochemical alterations in high-water-content biological matrices such as cartilage. These advantages position Raman spectroscopy as a powerful early-stage OA diagnosis and characterization technique [57].

3.3.1 | Comparative Analysis of Healthy and Grade 3 OA Cartilage

The Raman spectra acquired from both healthy and OA cartilage samples reveal distinct GAGs, hydroxyproline, proline, and C—H bending modes. In Grade 3 OA cartilage samples (Figure 7A), significant alterations were observed across most of these characteristic peaks, suggesting substantial structural and biochemical disruptions within the ECM and collagen network as OA advances. A marked reduction in amide I and amide III band intensity was particularly evident in OA-affected samples, indicative of collagen matrix degeneration, a key feature of ECM breakdown. Additionally, this attenuation reflects changes in the orientation and organization of collagen fibres, contributing to compromised mechanical integrity in OA cartilage. Prior studies have consistently identified this reduction in amide I intensity

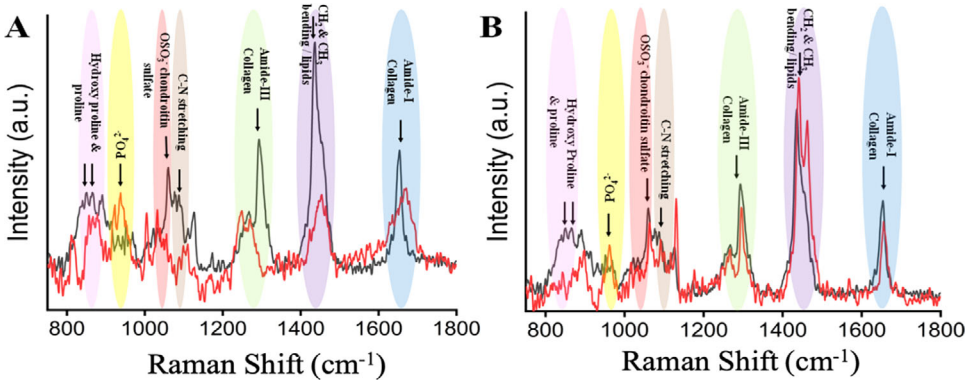

FIGURE 7 | (A) shows Raman spectra of healthy cartilage (black) and Grade 3 OA cartilage sample (red). (B) shows Raman spectra of healthy cartilage (black) and Grade 2 OA cartilage samples (red).

TABLE 2 | Raman Spectroscopic Analysis of Collagen and Glycosaminoglycan Components.

Raman Peak (cm^{-1})	Assignment
1657	Amide-I of collagen
1457	CH2 & CH3 bending mode associated with lipids/ collagen
1245-1300	Amide-III of Collagen
1063	Sulphated glycosaminoglycan
1079	C—N, C—C
953	PO_4^{2-}
857	Proline
879	Hydroxy Proline
815	C—C stretching of protein backbone

as a critical biomarker for OA progression, underscoring its potential utility in tracking molecular-level changes linked to cartilage degradation [56]. A notable characteristic observed in cartilage samples affected by OA is the absence of a significant reduction of the peak at 1063 cm^{-1}. This peak is associated with the O-SO_3^- stretching vibration of chondroitin sulphate found in GAGs within healthy cartilage. Its reduction or loss indicates proteoglycan depletion, a crucial marker of OA progression [58]. Furthermore, the spectral region ranging from 800 to 900 cm^{-1}, corresponding to the vibrational features of proline and hydroxyproline residues, exhibits marked changes in OA samples (Table 2). These alterations signal potential disruptions in collagen cross-linking or a decline in the stability of its helical structures, both essential for preserving the resilience and integrity of cartilage. The disappearance of the peak at 1079 cm^{-1}, associated with the C—O and C—N stretching vibrations from components in synovial fluid and articular cartilage, has been observed, which further corroborates with our other spectroscopy results [59]. Additionally, the emergence of a peak at 953 cm^{-1}, corresponding to the PO_4^{2-} stretching vibration, signals the onset of cartilage calcification as the disease progresses. This phosphate-associated peak indicates the mineralization of the cartilage matrix, a characteristic feature of advanced degeneration in OA [60].

3.3.2 | Comparative Analysis of Healthy and Grade 2 OA Cartilage

In the Grade 2 OA patient, spectral alterations were noted, however, these changes were less pronounced than those observed in Grade 3 OA patients. Unlike the advanced stage of the disease, the intensities of the amide I and amide III peaks did not exhibit significant reductions, indicating that these patients were likely in the earlier stages of OA progression. A slight decrease in the intensity of the peak at 1063 cm^{-1}, associated with the O-SO_3^- stretching of chondroitin sulphate found in GAGs, suggests a lower severity of disease at this stage. Additionally, the emergence of the PO_4^{2-} peak in Grade 2 patients indicates early calcification processes within the cartilage. The absence of peaks corresponding to hydroxyproline and proline at 857 and 879 cm^{-1}, respectively, reflects alterations in collagen cross-linking and the stability of α-helical structures. Furthermore, the observed reduction in the intensity of the C—N stretching vibration corroborates our previous findings, highlighting ongoing biochemical changes within the cartilage matrix (Figure 7B) [61].

3.4 | Quantitative Analysis of GAGs and Total Collagen Content in OA Cartilage

The ECM of cartilage is primarily composed of proteoglycans, where GAGs, including chondroitin sulphate and keratan sulphate, play a crucial role in maintaining the biomechanical properties of cartilage. These GAGs enabled cartilage to retain water, resist compressive forces, and maintain structural integrity [62]. In this study, we employed the DMMB assay, a colorimetric method widely recognized for its sensitivity and specificity in detecting sulphated GAGs, to quantify GAG concentrations in cartilage samples across various stages of OA. By examining healthy, Grade 2, and Grade 3 OA cartilage samples, the DMMB assay provided insights into the degree of ECM degradation at each stage, illustrating the progressive biochemical deterioration of cartilage with increasing OA severity. The results indicated a high GAG concentration of approximately 70% in healthy cartilage, reflecting a well-preserved ECM with balanced synthesis and degradation processes. In contrast, Grade 2 OA samples demonstrated a significant reduction in GAG content, measured at approximately 28% (Figure 8D). Noteworthy, the degradation became more pronounced in Grade 3 OA samples, where GAG

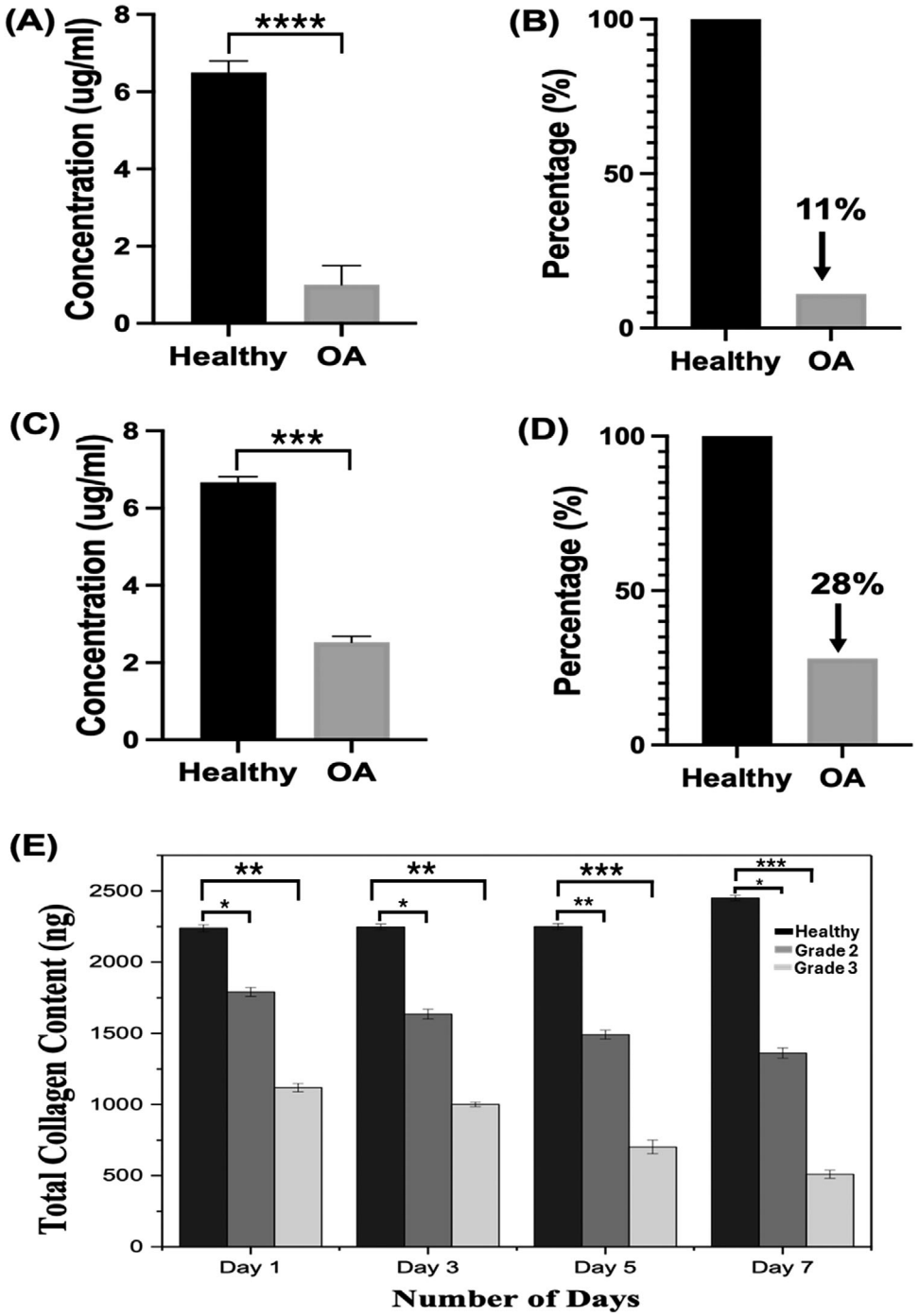

FIGURE 8 | Quantification of Glycosaminoglycan (GAG) concentration and its percentage distribution in healthy and osteoarthritic (OA) cartilage. (A) GAG concentration (μg/mL) in healthy cartilage compared to Grade 3 OA cartilage, showed a significant reduction in GAG levels in OA. (B) Percentage distribution of GAG in healthy cartilage vs. Grade 3 OA cartilage indicating severe ECM degradation. (C) GAG concentration (μg/mL) in healthy cartilage compared to Grade 2 OA cartilage, showed a reduction in GAG levels in OA. (D) Percentage distribution of GAG in healthy cartilage vs. Grade 2 OA cartilage highlighting ECM degradation. (E) Total collagen content of healthy, Grade 2 and Grade 3 OA cartilage. Data are expressed as average value ± SD (*$p < 0.05$, **$p < 0.01$).

content dropped to a critical level of around 11% (Figure 8B). The total collagen content was estimated to determine the extent of ECM present within the cartilage samples on day 1, 3, 5 and 7 (Figure 8E). An increase in collagen content was observed from day 1 to day 7 in the healthy cartilage samples. A decrease in collagen content was observed in Grade 2 and Grade 3 OA cartilage samples compared to the healthy cartilage samples. Surprisingly, a significant decline in collagen content was perceived in Grade 3 OA samples compared to Grade 2 samples and healthy cartilage samples on day 7.

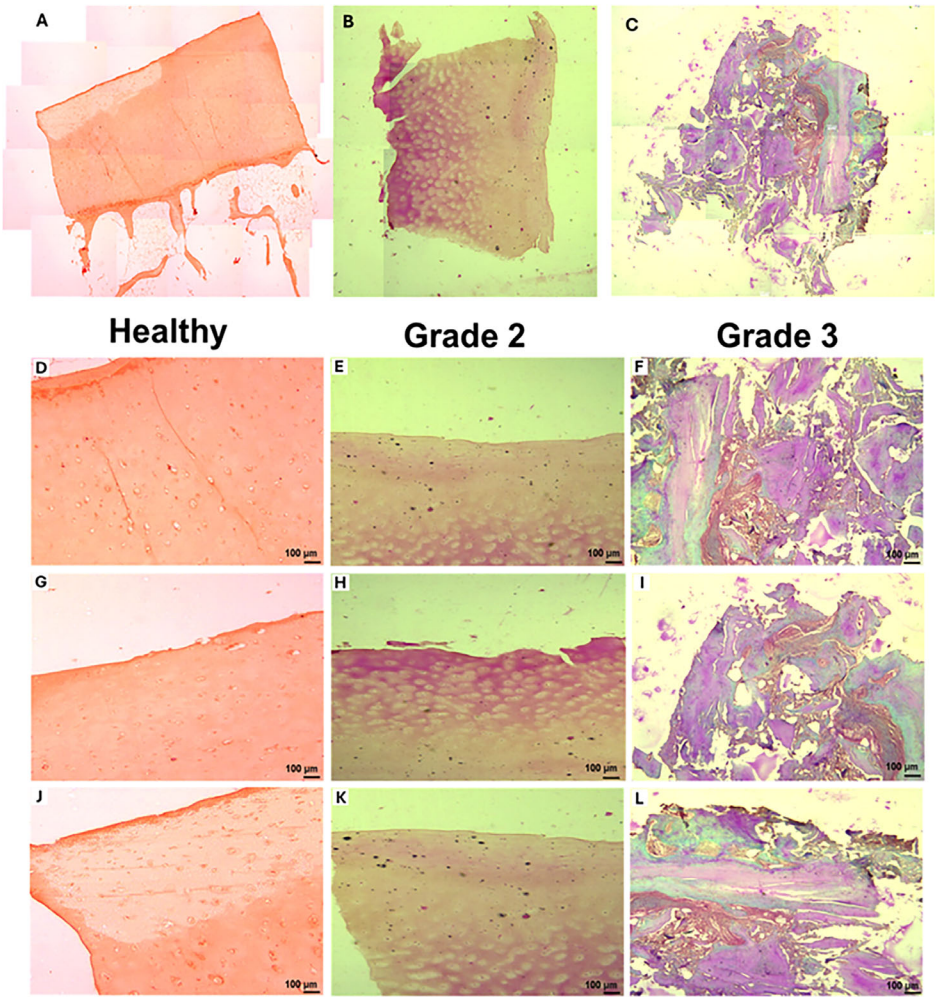

FIGURE 9 | Histological assessment of the main tissue samples (A–C) and corresponding tile images (D–L) stained with Safranin O. Panels A, B, and C represent the primary healthy, Grade 2, and Grade 3 cartilage samples, respectively. Tile images from additional sections show (D, G, J) healthy cartilage, (E, H, K) Grade 2 osteoarthritic cartilage, and (F, I, L) Grade 3 osteoarthritic cartilage. Healthy cartilage exhibits strong and uniform Safranin O staining, indicating abundant glycosaminoglycans and a well-preserved ECM. Grade 2 OA cartilage shows a notable reduction in Safranin O staining, particularly in the superficial and middle zones, with evidence of fibrillation and chondrocyte clustering. Grade 3 OA cartilage presents severe matrix degradation, with minimal Safranin O staining, extensive fibrillation, clefts, and hypertrophic chondrocytes, indicative of advanced osteoarthritic progression.

3.5 | Histological Analysis

Safranin-o staining was carried out to evaluate GAG distribution and ECM integrity in healthy, Grade 2, and Grade 3 OA cartilage (Figure 9). The staining intensity correlated with the severity of cartilage degeneration, reflecting progressive ECM disorganization and structural deterioration associated with OA. In healthy cartilage, a uniform and intense red-orange staining was observed throughout the ECM, indicative of a well-preserved proteoglycan-rich matrix. The chondrocytes were evenly distributed within distinct lacunae, and the articular surface appeared smooth and continuous, signifying an intact tissue structure. The homogeneous staining pattern suggested optimal cartilage hydration and biomechanical function [63]. In Grade 2 OA cartilage, a significant reduction in safranin-o staining intensity was observed, where the color shifted from red-orange to lighter red or pale regions. Large unstained areas were present, indicative of early proteoglycan depletion [64]. Structural alterations, including irregular chondrocyte clustering, initial fibrillation, and mild surface discontinuities, were evident. Compared to the healthy cartilage, the staining appeared more fragmented, with lighter red areas interspersed with unstained regions, reflecting the onset of ECM breakdown [65].

In Grade 3 OA cartilage, severe ECM degradation was evident, with a near-complete loss of safranin-o staining. The majority of the matrix appeared pale yellow to completely unstained, signifying extensive GAG depletion and loss of proteoglycan content. The tissue exhibited deep clefts, fibrillation, and severe fragmentation, with clear signs of fibrocartilage-like transformation. Notably, regions of intense purple and bluish staining were detected, particularly surrounding clusters of hypertrophic chondrocytes, which appeared enlarged and rounded, suggesting matrix mineralization and chondrocyte hypertrophy. The presence of fibrotic regions, along with extensive ECM disorganization, supports the hypothesis that OA progression involves not only proteoglycan loss but also compositional changes, including mineralization and fibrotic remodeling [63]. These findings confirm a progressive depletion of GAGs and increasing ECM disorganization as OA severity advances. The transition from

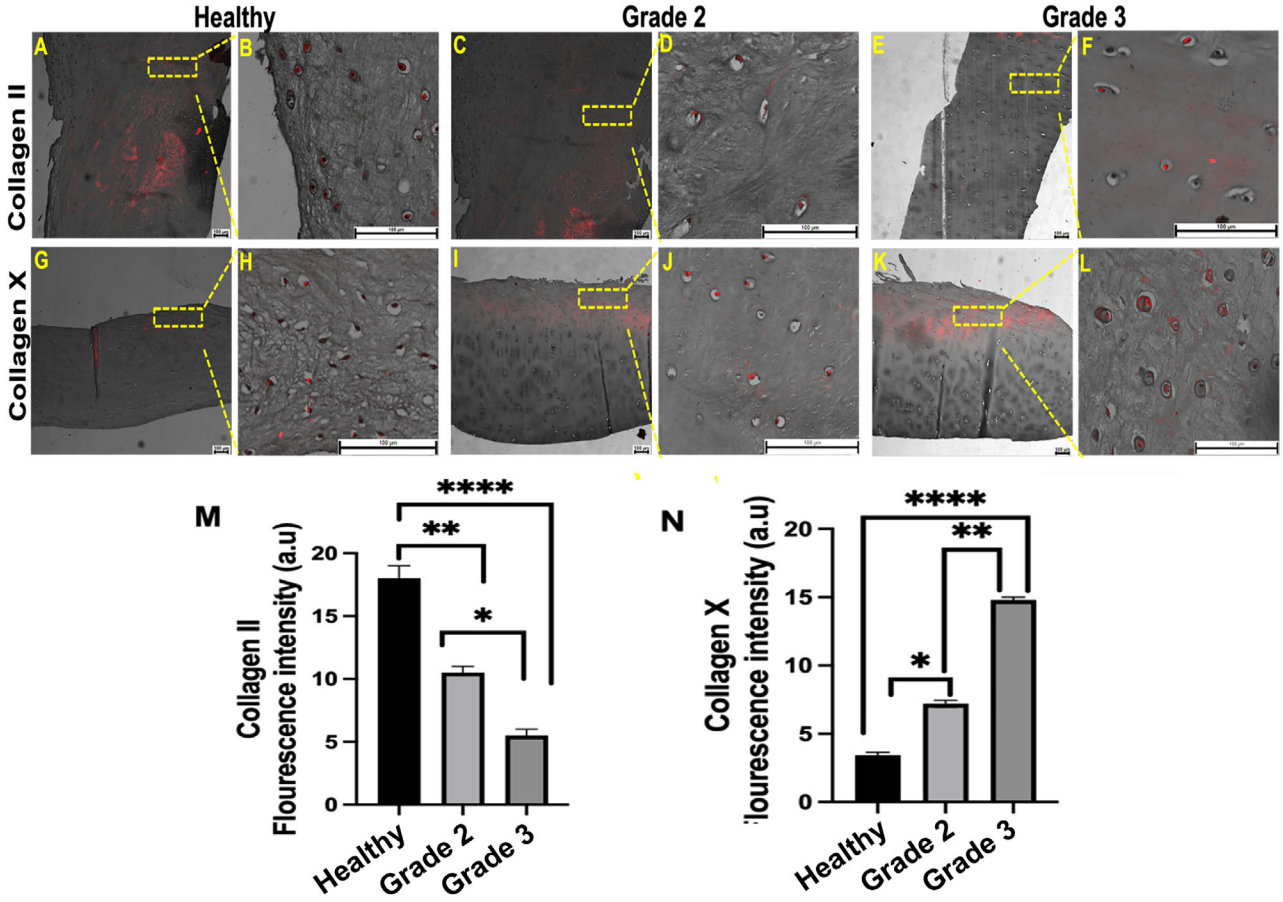

FIGURE 10 | Immunohistochemical detection of collagen II and X in human articular cartilage from healthy, Grade 2, and Grade 3 osteoarthritic samples. Panels A–F show collagen II staining, while panels G-L represent Collagen X staining. In healthy cartilage (A, B), collagen II is abundantly expressed throughout the ECM, with a progressive reduction observed in Grade 2 (C, D) and Grade 3 (E, F) OA tissues. In contrast, collagen X expression (G–L), a marker of chondrocyte hypertrophy, increases with OA severity. Red chromogen signal indicates positive staining. Images were acquired using a confocal microscope in brightfield mode. Scale bar = 100 μm. (M, N) Quantification of red fluorescence intensity (mean ± SD) reveals a significant decrease in collagen II and a corresponding increase in collagen X with OA severity. Statistical significance is denoted by $^{*}p < 0.05$, $^{**}p < 0.01$.

a proteoglycan-rich cartilage to a fibrocartilage-like phenotype, combined with chondrocyte hypertrophy and structural deterioration, underscores the role of matrix remodeling and cellular alterations in OA pathogenesis.

3.6 | Immunohistochemical Analysis of Cartilage ECM Remodeling and Hypertrophy in OA

Immunohistochemical staining of human articular cartilage samples revealed distinct and progressive alterations in the expression patterns of collagen II and collagen X across healthy, Grade 2, and Grade 3 OA conditions. All images were acquired using a confocal laser scanning microscope with excitation at 552 nm and overlaid with brightfield imaging to visualize tissue architecture. One of the main aims was to utilize the brightfield imaging method to facilitate a clear and exclusive detection of matrix-bound collagen signals (Figure 10).

In healthy cartilage, collagen II was abundantly and evenly distributed throughout the ECM, especially around the spaces housing chondrocytes, known as chondrocytic lacunae. This organized fibrillar network denotes the biochemical and structural integrity of hyaline cartilage, which is characterized by a dense matrix of collagen II interlinked with sulphated GAGs such as chondroitin sulphate and keratan sulphate. These interactions maintain cartilage osmotic pressure and resistance to compressive loading. In Grade 2 OA cartilage, a notable decrease in collagen II expression was observed. The ECM displayed regional discontinuities with fragmented and reduced collagen II signal, particularly in the territorial matrix. The decrease in signal intensity reflects catabolic ECM remodeling, driven by enzymatic degradation via matrix metalloproteinases (MMP-1, MMP-13) and aggrecanases (ADAMTS-4/5), resulting in collagen network disassembly and partial loss of GAG content. The pericellular matrix surrounding chondrocytes also appeared diminished, indicating early disruption of the chondrocyte microenvironment essential for mechanotransduction and matrix maintenance. In Grade 3 OA cartilage, collagen II expression was markedly diminished, with only sparse and punctate immunofluorescent signals localized to a few remaining chondrocytes. Both the territorial and interterritorial matrix zones exhibited near-complete loss of collagen II, reflecting widespread degradation of the fibrillar collagen network. This extensive matrix disruption signifies an advanced degenerative state characterized by sustained proteolytic activity, severe GAG depletion, and compromised biomechanical integrity

of the ECM. The resulting collapse of the collagen II architecture leads to a pathological transition from hyaline cartilage to a fibrotic and mineralized tissue phenotype, which lacks the essential viscoelastic properties required for normal joint load-bearing function.

Contrastingly, in healthy cartilage, the expression of collagen X was minimal to undetectable, reflecting the physiologically quiescent state of articular chondrocytes, which are terminally differentiated and non-hypertrophic under homeostatic conditions. Immunofluorescence analysis showed a near absence of collagen X staining, particularly in the mid and deep zones, indicating the lack of hypertrophic remodeling or mineralization, both of which are characteristic of disease-associated changes.

In Grade 2 OA cartilage, there was a moderate upregulation of collagen X, primarily localized in the pericellular regions of chondrocytes situated in the middle to deep cartilage zones. Morphologically, these cells began to exhibit early hypertrophic features, including mildly enlarged lacunae and increased cytoplasmic volume. Whereas, in Grade 3 OA, collagen X expression was significantly elevated and diffusely distributed throughout the cartilage matrix. Confocal overlay images revealed intense collagen X fluorescence surrounding large groups of hypertrophic chondrocytes, many of which displayed enlarged and irregular lacunae and dense pericellular collagen X accumulation.

A multimodal validation of GAG depletion across OA grades using six techniques was also conducted (Figure S1): XPS, FTIR, Raman spectroscopy, DMMB assay, Safranin-O histology, and IHC for Collagen II/X. Panel A shows the relative decline in GAG content from Healthy to Grade 3 cartilage, derived from spectroscopic analyses processed in OriginPro 2023b, biochemical measurements obtained using the DMMB assay, and quantitative image intensity analysis performed in ImageJ for histology and IHC images. All histology and IHC images were captured using a Leica bright-field microscope and confocal imaging system under identical acquisition settings. Panel B displays the correlation heatmap generated in GraphPad Prism 9, demonstrating strong inter-method agreement ($r = 0.94–1.00$). Together, these analyses confirm that GAG loss is consistently detected across all modalities and serves as a robust and reliable marker of OA progression.

4 | Discussion

A large section of the general population suffers from age-related OA. They show symptoms of a displaced endochondral ossification. Reactivation of this program is evidenced a framework of pleiotropic antagonism. The cartilage ECM can be probed using label-free characterisation methods such as second harmonic generation, and infrared and near-infrared spectroscopy [66]. All of these methods can only, however, examine changes in a semi-quantitative manner. Hence, to overcome this limitation, we have employed XPS, which is especially useful for investigating biologically significant interfaces, such as protein layers and biomaterials, and offers accurate chemical composition at the nanoscale [67]. Therefore, in order to investigate the remodeling of the articular cartilage at various stages of OA, two samples of OA patients, categorized as Grade 2 and Grade 3, were obtained and compared with a sample of healthy cartilage using advanced spectroscopic approaches. XPS provides surface-sensitive detection of elemental composition, elucidating variations in sulphur and nitrogen contents associated with GAGs and collagen [68].

In comparison to the study by Jaabar et al. [68] which also employed XPS to analyse cartilage ECM changes during OA progression, our approach offered enhanced precision and depth in detecting chemical alterations. While both studies used XPS to evaluate ECM composition, Jaabar et al.'s method primarily focused on tracking changes in aggrecan and collagen content during different stages of OA [68]. They reported an initial increase in aggrecan and collagen concentrations in the early-to-middle stages of OA, followed by a significant decrease as the disease advanced. Our study, on the other hand, emphasized the chemical state of ECM elements, such as the nitrogen and carbon atoms within collagen and GAGs. The presence of the nitrogenous elements in a healthy cartilage sample suggested a strong ECM composition, with GAGs playing a critical role in hydration, elasticity, and compressive resilience. This nitrogen signal, alongside the carbon peak at 285 eV and the oxygen peak at 532 eV, further confirmed a substantial presence of GAGs and collagen, indicating a structurally intact and functionally robust ECM [49].

Contrastingly, the complete absence of the nitrogen peak at 399 eV in the Grade 3 OA sample was especially striking, suggesting a near-total depletion of nitrogen-rich components, including GAGs and collagen. This absence was a critical indicator of a diminished GAG concentration, as GAGs were primarily responsible for the nitrogen signal in the ECM [69]. Additionally, the reductions in the carbon and oxygen signals further indicated a breakdown of glycosidic bonds in GAGs and peptide bonds in collagen, which contributed to the ECM's structural framework [70]. Without the nitrogenous and oxygen-rich GAGs, the ECM lost its capacity to maintain the critical balance of hydration and elasticity that supported joint function. Consequently, the diminished GAG concentration in Grade 3 OA cartilage impaired the tissue's biomechanical properties, contributing to joint stiffness, reduced shock absorption, and increased vulnerability to mechanical damage, ultimately exacerbating the clinical progression of OA. On the other hand, the reduction in the nitrogen signal in Grade 2 OA in patient 2 sample suggested a partial degradation of nitrogen-rich ECM components, indicating that the concentrations of GAGs and collagen had begun to decline due to the progression of the OA process. Although these decreases in carbon, nitrogen and oxygen peaks were less pronounced than those observed in Grade 3 OA cartilage, the moderate decline in the carbon peak suggested a minute level of degradation in the organic compounds present in the ECM, including the carbon backbones of GAGs. This finding implied that while GAGs were still present in the cartilage, their overall concentration was reduced, contributing to the compromised structural integrity of the tissue. Similarly, the oxygen peak, associated with oxygen-containing functional groups such as hydroxyl, carboxyl, and amide groups, also exhibited a reduction in intensity. The observed reductions in the intensity of the nitrogen-containing groups in the Grade 2 OA cartilage indicated that, although GAGs and collagen were still detectable, their overall quantities were diminished compared to healthy cartilage. This partial degradation suggested an early stage of

the disease, characterized by the initiation of the loss of critical ECM components necessary for proper cartilage function. The moderate decreases in both the carbon and oxygen peaks further supported the conclusion that there had been a partial loss of GAGs and collagen in Grade 2 OA cartilage, aligning with the clinical observations of patient 2, who exhibited moderate ECM degradation but had not yet reached the severe degeneration characteristic of advanced OA stages, such as those seen in Grade 3 samples.

Jaabar et al. [68] mentioned the presence of hydrocarbon contamination in their XPS data, likely from biological lipids, but did not address this issue as thoroughly as our method, which involved cryogenic milling and surface sputtering to remove adsorbed hydrocarbons. This step was critical in ensuring that the observed changes in nitrogen and carbon concentrations were reflective of actual ECM degradation rather than external contaminants. The XPS analysis thus underscored the stark biochemical differences between healthy and OA cartilage, highlighting the loss of nitrogen and other ECM components as fundamental indicators of cartilage degradation in patient 1's Grade 3 OA.

Understanding cartilage degradation in diseases like OA and assessing the efficacy of cartilage repair techniques are two areas in which this technology is especially helpful [71]. The reduced intensity of the nitrogen peak in the Grade 2 OA sample in the FTIR spectra indicated that some degradation of the cartilage had occurred, but important components of the ECM remained intact. These findings were supported by the carbon spectrum analysis, which also showed a decrease in carbon-nitrogen (C—N) bonding, though not as significant as in Grade 3 OA samples [50]. Collagen II is the principal structural protein in articular cartilage, forming a dense, cross-linked meshwork that resists tensile and shear forces. The reduced spectral intensity at 1337 cm^{-1} indicates disruption of the triple-helical structure and fragmentation of collagen fibres, which weakens the biomechanical stability of the ECM. As a result, the tissue becomes more prone to damage during joint movement, an early sign of OA progression. Overall, the reduced intensities of the GAG (1385 cm^{-1}), amide II (1537 cm^{-1}), and collagen II (1337 cm^{-1}) peaks reflect early ECM disintegration in Grade 2 cartilage. The partial depletion of GAGs and collagen suggests compromised mechanical integrity and hydration capacity. These findings point out to the fact that in the early stages of OA, there still may have some opportunities for interventions that could help maintain cartilage structure and function. Focusing on preserving GAG concentration in Grade 2 OA could have been crucial in slowing the progression of the disease, setting it apart from the more advanced degenerative changes observed in Grade 3 OA [72]. Taken together, the ATR-FTIR findings corroborate the results from XPS analysis, which also demonstrated a decline in ECM-related elemental signals, validating progressive biochemical degradation at this stage [73].

Similar results were obtained by Raman Spectroscopy that enhances ATR-FTIR results by detecting shifts in molecule vibrations, explaining nuanced changes in GAG and collagen structure during the OA progression [17, 58]. This was according to the study by Power et al. [74], where they reported the efficacy of Raman spectroscopy as a proof-of-concept to ascertain the tissue types in nasal septal biopsy. The tissues were categorised with a sensitivity of 89% and a specificity of 77%. They demonstrated the assessment of clinically relevant and mature nasal chondrocyte-derived synthetic cartilage using Raman spectroscopy for the creation of potency testing.

Histological analysis provides a structural assessment of cartilage degeneration, supporting the spectroscopic findings and linking the biochemical changes to tissue integrity loss. It further corroborated the spectroscopic findings, demonstrating progressive ECM disorganization, proteoglycan depletion, and chondrocyte hypertrophy. By deconvoluting XPS spectra, we identified specific bonding changes, such as the depletion of nitrogen-rich amide groups in collagen, providing a more in-depth understanding of ECM breakdown mechanisms and the decrease or absence of GAG concentration. Histological analysis further reinforced these findings by showing a reduction in safranin-o staining intensity, particularly in Grade 3 OA samples, highlighting advanced cartilage degradation. The ability of cartilage to resist compressive stresses and preserve joint lubrication depends on sulphated GAGs, which are important molecules of the cartilage ECM [41, 75]. The pronounced reduction in GAG content between Grades 2 and 3 OA indicated a pivotal threshold where biochemical degradation progressed into irreversible structural damage, ultimately compromising joint functionality [72]. These changes were also accompanied by significant morphological alterations, including cartilage thinning, subchondral bone sclerosis, and osteophyte formation, characteristic of late-stage OA [25]. The findings from this study underscored the value of the DMMB assay in quantitatively assessing GAG content as an indicator of ECM integrity. From a therapeutic perspective, our study suggested the importance of early intervention strategies that focused on preserving or enhancing GAG synthesis, which could potentially delay or mitigate the advancement of OA. To further validate these observations at the cellular level, immunohistochemical staining was also performed to assess the expression of collagen II and Type X across healthy and OA cartilage. This allowed us to spatially map ECM changes and hypertrophic differentiation, strengthening the link between biochemical degradation and phenotypic transformation in OA chondrocytes. The terminal hypertrophic differentiation is pathologically inappropriate for articular cartilage and plays a critical role in driving OA progression [76]. The growth plates, the calcified layer of articular cartilage, several skeletal structures, and the healing process of fractures all contain hypertrophic chondrocytes. In terms of appearance, hypertrophic chondrocytes are defined as larger chondrocytes. They express Col 10A1 in particular, which codes for type X collagen, a crucial indicator of hypertrophic chondrocytes [9]. Hypertrophic chondrocytes, unlike their healthy counterparts, actively express collagen X, along with matrix-degrading enzymes such as MMP 13 and ADAMTS-5, which contribute to the breakdown of collagen II in the ECM region. The presence of collagen X-positive hypertrophic chondrocytes in advanced OA reflects a transition from a maintenance phenotype to a destructive, remodeling state, which significantly contributes to irreversible cartilage degeneration, fibrocartilage formation, and joint dysfunction. The significant expression of collagen X as ascertained from immunohistochemistry results in Grade 2 and 3 OA samples, appears to precede overt matrix degradation, suggesting that hypertrophic differentiation may actively contribute to ECM destabilization. This pattern of expression suggests the initiation of a hypertrophic differentiation program, likely mediated by the RUNX2–COL 10A1 signalling axis, a

key regulator of chondrocyte maturation. Similar to our study Hatton et al. [77] employed XPS to characterize alginate-based hydrogels functionalized through layer-by-layer assembly, identifying surface biomolecule incorporation. However, their analysis relied solely on surface-level composition without addressing adsorbed contaminants or performing depth profiling, as evidenced by their focus on elemental detection without mitigation of hydrocarbon interference.

While their study utilized animal cartilage, specifically bovine articular chondrocytes (BAC) from skeletally mature beef cattle, our approach focused on human cartilage, ensuring direct relevance to OA disease progression in humans. In contrast, our approach utilized cryogenic milling and argon-ion sputtering to eliminate surface contamination, coupled with high-resolution spectral deconvolution, enabling precise identification of ECM-specific chemical state alterations, such as nitrogen-rich amide group depletion in collagen. These enhancements ensured greater accuracy and depth in analysing cartilage degeneration pathways. In addition, the increased expression of collagen X detected via IHC in the Grade 3 OA sample provided crucial evidence of chondrocyte hypertrophy, which is a key driver of matrix degradation that aligns with our hypothesis and ATR-FTIR finding. The findings demonstrate a strong relationship between chondrocyte hypertrophy and ECM degradation in OA cartilage. The increased expression of hypertrophic markers, along with the loss of GAG and collagen organization, supports the role of hypertrophy in driving ECM remodeling. Consistent with previous in vitro and animal studies by Chawla et al. [79] and Majumder et al. [17] which showed that hypertrophic differentiation activates matrix-degrading enzymes such as MMP-13 and ADAMTS-5, our results provide human-tissue evidence that hypertrophy contributes to ECM disorganization and may represent an upstream event in osteoarthritis progression.

Our combined spectroscopic methods provided a more detailed and precise molecular analysis of cartilage degeneration. This study, on another side, validated our hypothesis from previous studies specifically, the findings from Chakraborty et al. [78], Chawla et al. [79], and Majumder et al. [17]. that chondrocyte hypertrophy leads to the progression of OA by altering GAG and collagen concentrations. Our focus was on chemical state analysis, and the use of multiple techniques enabled us to capture a broader range of biochemical changes for two different conditions, particularly in relation to GAG and collagen depletion. By integrating histological analysis, we confirmed the progressive loss of GAGs, collagen disorganization, and chondrocyte hypertrophy, emphasizing the critical role of structural changes in OA pathogenesis.

To further support these findings, we qualitatively compared trends observed across all analytical techniques. The reduction in GAG levels measured by the DMMB assay showed a similar pattern to the decrease in nitrogen- and amide-related signals detected by XPS and ATR-FTIR, respectively. Likewise, attenuation of the GAG-specific Raman peak (~1063 cm^{-1}) aligned with the reduced Safranin-O staining seen histologically. This consistent trend across spectroscopic, biochemical, and histological methods indicates strong concordance between techniques, reinforcing the reliability of GAG depletion as an indicator of ECM degradation during OA progression. While several previous studies have analysed OA-related biochemical changes using animal models such as rats, our study is distinguished by its rigorous investigation of human cartilage samples.

The number of patient samples in this study was limited. The work was conceived as a pilot, proof-of-concept investigation aimed at developing and validating a reproducible, multimodal analytical framework that integrates spectroscopic, biochemical, and histological assessments of human cartilage. This approach enabled the identification of consistent molecular signatures of GAG depletion, collagen disorganization, and hypertrophic transformation, even within a small cohort. Building on this foundation, the next phase of our research will include a larger and clinically diverse patient population to strengthen the statistical significance of these findings and to identify additional biochemical, biomechanical, histological and signalling parameters that will further elucidate the role of cartilage hypertrophy in OA progression and enhance translational relevance.

The present work introduces a distinctive methodological and conceptual advancement in the study of OA cartilage. By integrating surface-sensitive (XPS) and vibrational (ATR-FTIR and Raman) spectroscopic analyses with biochemical quantification (DMMB and hydroxyproline assays) and histological validation, this study provides a comprehensive molecular-to-tissue scale characterization of ECM deterioration in human OA cartilage. Unlike most earlier investigations that relied on animal or in vitro models, the direct assessment of patient-derived cartilage offers clinically relevant molecular signatures of GAG depletion, collagen disorganization, and hypertrophic transformation. One of the major challenges in managing OA is its late detection. Early-stage OA is far more responsive to conservative or biological therapies, whereas late-stage disease often leaves joint replacement as the only option. Clinically, early OA often presents with minimal pain, limited structural damage, and subtle biomechanical alterations, making it difficult to diagnose. In this context, our findings help clarify whether OA reflects a modified reactivation of endochondral ossification. The combined depletion of GAGs, increased MMP-13 expression, appearance of collagen type X, and progressive ECM disorganization closely mirror the hypertrophic and matrix-remodeling events characteristic of endochondral bone formation. Their co-occurrence in OA cartilage supports the view that OA is not merely a degenerative "wear-and-tear" condition, but a maladaptive reactivation of ossification-like pathways triggered by inflammation and mechanical stress. Recognizing these early molecular deviations emphasizes the need for sensitive early-diagnostic tools. Our group has contributed to this direction through AI-based approaches across different disease stages: an early-stage histological classifier by Nagarajan et al. [65] and an MRI-based deep-learning model developed by Roy et al. to determine OA severity directly from patient MRI scans [80]. Building on this computational foundation, the present multimodal biochemical–structural analysis provides direct molecular evidence—such as early GAG loss, ECM disruption, and hypertrophic marker upregulation—that supports and strengthens the predictive patterns identified by our AI models.

5 | Conclusion

Explaining OA as an "evolutionary and biological program" is a new and upcoming theory of "cartilage wear and tear". This

study analysed the human cartilage degradation in OA through a grade-based biochemical and molecular approach. In Grade 3 OA, observed in patient 1, aged 66, advanced and pronounced osteophyte formation significantly disrupted cartilage integrity by reducing thickness and damaging the cartilage lining. This structural damage resulted in a severe depletion of GAGs, with concentrations decreasing to approximately 11% ($p < 0.05$). A significant reduction in ECM components, including collagen concentrations was observed. Molecular analysis using XPS confirmed the absence of nitrogen-rich amide groups and glycosidic bonds, while ATR-FTIR revealed diminished amide II peaks, further highlighting advanced ECM disorganization and the loss of cartilage functionality associated with late-stage OA. Histological analysis using Safranin O staining further validated these findings, showing severe depletion of GAGs, extensive matrix disorganization, and hypertrophic chondrocytes, which are indicative of cartilage mineralization and structural failure. Additionally, immunohistochemical analysis revealed a marked loss of collagen II and a strong upregulation of collagen X in Grade 3 OA, confirming the occurrence of terminal hypertrophic chondrocyte differentiation and its role in matrix breakdown. In Grade 2 OA, observed in patient 2, aged 57, smaller osteophytes indicated the early phase of cartilage degeneration. Structural alterations began to compromise cartilage thickness, providing early signs of disease progression. GAG concentrations were reduced to approximately 28% ($p < 0.05$). Moderate collagen disorganization was evident. These findings were supported by ATR-FTIR, which showed reduced glycosidic peaks, and Raman spectroscopy, which revealed early structural alterations in ECM components. Histological analysis further supported these biochemical findings, revealing a moderate reduction in Safranin O staining intensity, indicating early GAG depletion. Additionally, signs of pericellular matrix expansion, initial fibrillation, and early-stage vascular invasion were observed, marking a critical transition where ECM degradation processes are initiated, signalling the progression toward Grade 3 OA. Immunohistochemical staining in Grade 2 OA samples also demonstrated moderate collagen II depletion and the onset of collagen X expression around middle to deep zone chondrocytes, suggesting early hypertrophic transition associated with matrix destabilization. Characterization techniques, including XPS, ATR-FTIR, Raman spectroscopy, DMMB assay, hydroxyproline assay, immunohistochemistry and histological analysis, collectively validated the biochemical and molecular findings, providing a comprehensive understanding of cartilage degeneration. Our study demonstrates a clear correlation between osteophyte formation, ECM degradation, and cartilage dysfunction across different Grades of OA. GAG and hydroxyproline concentration as assessed from the total collagen concentration served as a biomarker for disease progression, providing a foundation for developing Grade-specific diagnostic and therapeutic strategies targeting ECM stabilization in OA.

Acknowledgements

The authors would like to acknowledge Apollo Hospitals Indraprastha, New Delhi, India for their support in providing the human tissue samples for our study.

Conflicts of Interest

The authors declare no conflicts of interest.

Data Availability Statement

The data that support the findings of this study are available on request from the corresponding author. The data are not publicly available due to privacy or ethical restrictions.

References

1. T. Neogi, "The Epidemiology and Impact of Pain in Osteoarthritis," *Osteoarthritis and Cartilage* 21, no. 9 (2013): 1145–1153.

2. M. Hall, M. van der Esch, R. S. Hinman, et al., "How Does Hip Osteoarthritis Differ From Knee Osteoarthritis?," *Osteoarthritis and Cartilage* 30, no. 1 (2022): 32–41.

3. J. Chakraborty, J. Fernandez-Perez, M. T. Ghahfarokhi, et al., "Development of 4D-bioprinted Shape-morphing Magnetic Constructs for Cartilage Regeneration Using a Silk Fibroin-gelatin Bioink," *Cell Reports Physical Science* 5, no. 3 (2024): 101819.

4. Y. He, Z. Li, and P. G. Alexander, "Pathogenesis of Osteoarthritis: Risk Factors, Regulatory Pathways in Chondrocytes, and Experimental Models," *Biology* 9 (2020): 194.

5. G. Musumeci, F. C. Aiello, M. A. Szychlinska, M. D. Rosa, P. Castrogiovanni, and A. Mobasheri, "Osteoarthritis in the XXIst Century: Risk Factors and Behaviours That Influence Disease Onset and Progression," *International Journal of Molecular Sciences* 16 (2015): 6093–6112.

6. D. Shi, A. Sheng, and L. Chi, "Glycosaminoglycan-Protein Interactions and Their Roles in Human Disease," *Frontiers in Molecular Biosciences* 8 (2021): 639666.

7. A. H. Conrad, Y. Zhang, E. S. Tasheva, and G. W. Conrad, "Proteomic Analysis of Potential Keratan Sulfate, Chondroitin Sulfate A, and Hyaluronic Acid Molecular Interactions," *Investigative Opthalmology & Visual Science* 51 (2010): 4500–4515.

8. S. Chawla, A. Mainardi, N. Majumder, et al., "Chondrocyte Hypertrophy in Osteoarthritis: Mechanistic Studies and Models for the Identification of New Therapeutic Strategies," *Cells* 11 (2022): 4034.

9. P. M. van der Kraan, "Osteoarthritis as an Evolutionary Legacy: Biological Ageing and Chondrocyte Hypertrophy," *Osteoarthritis and Cartilage Open* 7 (2025): 100624.

10. S. Murab, S. Chameettachal, M. Bhattacharjee, S. Das, D. L. Kaplan, and S. Ghosh, "Matrix-embedded Cytokines to Simulate Osteoarthritis-Like Cartilage Microenvironments," *Tissue Engineering Part A* 19 (2013): 1733–1753.

11. T. A. E. Ahmed and M. T. Hincke, "Strategies for Articular Cartilage Lesion Repair and Functional Restoration," *Tissue Engineering Part B: Reviews* 16 (2010): 305–329.

12. J. Sokolove and C. M. Lepus, "Role of Inflammation in the Pathogenesis of Osteoarthritis: Latest Findings and Interpretations," *Therapeutic Advances in Musculoskeletal Disease* 5 (2013): 77–94.

13. M. C. Catoira, L. Fusaro, D. Di Francesco, M. Ramella, and F. Boccafoschi, "Overview of Natural Hydrogels for Regenerative Medicine Applications," *Journal of Materials Science: Materials in Medicine* 30 (2019): 115.

14. K. Kansara, A. Mansuri, A. Kumar, and D. Bhatia, "DNA Nano-Biomaterials Based Futuristic Technologies for Tissue Engineering and Regenerative Therapeutics," *Small* 21 (2025): 2504361.

15. S. Chawla, A. Kumar, P. Admane, A. Bandyopadhyay, and S. Ghosh, "Elucidating Role of Silk-gelatin Bioink to Recapitulate Articular Cartilage Differentiation in 3D Bioprinted Constructs," *Bioprinting* 7 (2017): 1–13.

16. S. Chameettachal, S. Midha, and S. Ghosh, "Regulation of Chondrogenesis and Hypertrophy in Silk Fibroin-Gelatin-Based 3D Bioprinted Constructs," *ACS Biomaterials Science & Engineering* 2 (2016): 1450–1463.

17. N. Majumder, C. Roy, L. Doenges, I. Martin, A. Barbero, and S. Ghosh, "Covalent Conjugation of Small Molecule Inhibitors and Growth Factors to a Silk Fibroin-Derived Bioink to Develop Phenotypically Stable 3D Bioprinted Cartilage," *ACS Applied Materials & Interfaces* 16 (2024): 9925–9943.

18. J. Chakraborty, N. Majumder, A. Sharma, S. Prasad, and S. Ghosh, "3D Bioprinted silk-reinforced Alginate-Gellan Gum Constructs for Cartilage Regeneration," *Bioprinting* 28 (2022): 00232.

19. Z. Deng, X. Chen, Z. Lin, et al., "The Homeostasis of Cartilage Matrix Remodeling and the Regulation of Volume-Sensitive Ion Channel," *Aging and Disease* 13 (2022): 787–800.

20. L. T. Ho, A. M. Harris, H. Tanioka, et al., "A Comparison of Glycosaminoglycan Distributions, Keratan Sulphate Sulphation Patterns and Collagen Fibril Architecture From central to Peripheral Regions of the Bovine Cornea," *Matrix Biology* 38 (2014): 59.

21. J. Katta, T. Stapleton, E. Ingham, Z. M. Jin, and J. Fisher, "The Effect of Glycosaminoglycan Depletion on the Friction and Deformation of Articular Cartilage," *Proceedings of the Institution of Mechanical Engineers, Part H: Journal of Engineering in Medicine* 222 (2008): 1–11.

22. A. Berdiaki, M. Neagu, P. Tzanakakis, I. Spyridaki, S. Pérez, and D. Nikitovic, "Extracellular Matrix Components and Mechanosensing Pathways in Health and Disease," *Biomolecules* 14 (2024): 1186.

23. N. Majumder, S. Seit, N. S. Bhabesh, and S. Ghosh, "An Advanced Bioconjugation Strategy for Covalent Tethering of TGFβ3 With Silk Fibroin Matrices and Its Implications in the Chondrogenesis Profile of Human BMSCs and Human Chondrocytes: A Paradigm Shift," *Cartilage Tissue Engineering* 13 (2024): 2303513.

24. M. D. Kohn, A. A. Sassoon, and N. D. Fernando, "Classifications in Brief: Kellgren-Lawrence Classification of Osteoarthritis," *Clinical Orthopaedics & Related Research* 474 (2016): 1886.

25. G. Li, J. Yin, J. Gao, et al., "Subchondral Bone in Osteoarthritis: Insight Into Risk Factors and Microstructural Changes," *Arthritis Research & Therapy* 15 (2013): 223.

26. A. Abazari, N. M. Jomha, J. A. Elliott, and L. E. McGann, "Cryopreservation of Articular Cartilage," *Cryobiology* 66, no. 3 (2013): 201–209.

27. W. J. McCarty, A. L. Pallante, R. J. Rone, W. D. Bugbee, and R. L. Sah, "The Proteoglycan Metabolism of Articular Cartilage in Joint-scale Culture," *Tissue Engineering Part A* 16, no. 5 (2010): 1717–1727.

28. A. Molnar, T. Lakat, A. Hosszu, et al., "Lyophilization and Homogenization of Biological Samples Improves Reproducibility and Reduces Standard Deviation in Molecular Biology Techniques," *Amino Acids* 53 (2021): 917–928.

29. M. Dixit, A. G. Kini, and P. K. Kulkarni, "Preparation and Characterization of Microparticles of Piroxicam by Spray Drying and Spray Chilling Methods," *Research in Pharmaceutical Sciences* 5 (2010): 89.

30. A. M. Hitchcock, K. E. Yates, S. Shortkroff, C. E. Costello, and J. Zaia, "Optimized Extraction of Glycosaminoglycans From Normal and Osteoarthritic Cartilage for Glycomics Profiling," *Glycobiology* 17 (2006): 25–35.

31. Z. Cao, Y. Liu, and J. Zhao, "Efficient Discrimination of some Moss Species by Fourier Transform Infrared Spectroscopy and Chemometrics," *Journal of Spectroscopy* 2014, no. 1 (2014): 191796.

32. A. Boskey and N. P. Camacho, "FT-IR Imaging of Native and Tissue-Engineered Bone and Cartilage," *Biomaterials* 28 (2006): 2465–2478.

33. S. L. McArthur, G. Mishra, and C. D. Easton, "Applications of XPS in Biology and Biointerface analysis," *Surface Analysis and Techniques in Biology* (Springer International Publishing, 2014), 9–36.

34. J. Daughtry, A. S. Alotabi, L. Howard-Fabretto, and G. G. Andersson, "Composition and Properties of RF-sputter Deposited Titanium Dioxide Thin Films," *Nanoscale Advances* 3 (2020): 1077–1086.

35. L. Gong, D. Alamarguy, N. Ruscassier, P. Haghi-Ashtiani, and M. L. Giorgi, "Understanding of Selective Oxidation of Fe-Mn Binary Alloys During Continuous Annealing Through X-ray Photoelectron Spectroscopy," *Corrosion Communications* 11 (2023): 72–82.

36. K. Hashimoto, V. R. Badarla, A. Kawai, and T. Ideguchi, "Complementary Vibrational Spectroscopy," *Nature Communications* 10 (2019): 4411.

37. T. Rojalin, T. L. L. Kurki, T. Viitala, J. Kostamovaara, K. Gordon, and M. C. Yliperttula, "Fluorescence-suppressed Time-resolved Raman Spectroscopy of Pharmaceuticals Using Complementary Metal-oxide Semiconductor (CMOS) Single-photon Avalanche Diode (SPAD) Detector," *Analytical and Bioanalytical Chemistry* 408, no. 3 (2016): 761–774.

38. K. Jurowski, M. Noga, D. Kobylarz, Ł. Niżnik, and A. Krośniak, "Multimodal Imaging Using Raman Spectroscopy and FTIR in a Single Analytical Instrument With a Microscope (Infrared Raman Microscopy AIRsight, Shimadzu): Opportunities and Applications," *International Journal of Molecular Sciences* 25 (2024): 6884.

39. F. Kubaski, H. Osago, R. W. Mason, et al., "Glycosaminoglycans Detection Methods: Applications of Mass Spectrometry," *Molecular Genetics and Metabolism* 120 (2016): 67–77.

40. C. Hoemann, "Molecular and Biochemical Assays of Cartilage Components," *Methods in Molecular Medicine* 101 (2004): 127–156.

41. V. J. Coulson-Thomas and T. F. Gesteira, "Dimethylmethylene Blue Assay (DMMB)," *Bio-Protocol* 4, no. 18 (2014): e1236–e1236.

42. Y. D. Ladner, M. Alini, and A. R. Armiento, "The Dimethylmethylene Blue Assay (DMMB) for the Quantification of Sulfated Glycosaminoglycans," *Cartilage Tissue Engineering* (Springer, 2022), 115–121.

43. Y. Xia, S. Zheng, and A. Bidthanapally, "Depth-Dependent Profiles of Glycosaminoglycans in Articular Cartilage by μMRI and Histochemistry," *Journal of Magnetic Resonance Imaging* 28 (2008): 151–157.

44. N. Y. Ignat'eva, N. A. Danilov, S. V. Averkiev, M. V. Obrezkova, V. V. Lunin, and E. N. Sobol', "Determination of Hydroxyproline in Tissues and the Evaluation of the Collagen Content of the Tissues," *Journal of Analytical Chemistry* 62 (2007): 51–57.

45. A. Alibegović, R. Blagus, and I. Z. Martinez, "Safranin O Without Fast Green Is the Best Staining Method for Testing the Degradation of Macromolecules in a Cartilage Extracellular Matrix for the Determination of the Postmortem Interval," *Forensic Science, Medicine and Pathology* 16 (2020): 252–258.

46. D. R. Pedersen, J. E. Goetz, G. L. Kurriger, and J. A. Martin, "Comparative Digital Cartilage Histology for human and Common Osteoarthritis Models," *Orthopedic Research and Reviews* 5 (2013): 13–20.

47. A. J. S. Fox, A. Bedi, and S. A. Rodeo, "The Basic Science of Articular Cartilage: Structure, Composition, and Function," *Sports Health* 1 (2009): 461.

48. J. C. Silva, M. S. Carvalho, X. Han, et al., "Compositional and Structural Analysis of Glycosaminoglycans in Cell-derived Extracellular Matrices," *Glycoconjugate Journal* 36 (2019): 141–154.

49. X. Chen, X. Wang, and D. Fang, "A Review on C1s XPS-spectra for some Kinds of Carbon Materials," *Fullerenes, Nanotubes and Carbon Nanostructures* 28 (2020): 1048–1058.

50. C. Tang, B. D. Holt, Z. M. Wright, A. M. Arnold, A. C. Moy, and S. A. Sydlik, "Injectable Amine Functionalized Graphene and Chondroitin Sulfate Hydrogel With Potential for Cartilage Regeneration," *Journal of Materials Chemistry B* 7 (2019): 2442–2453.

51. Q. Wu, J. Wu, L. Huang, et al., "In Situ Study on Articular Cartilage Degeneration in Simulated Microgravity by HOF-ATR-FTIR Spectroscopy," *Spectrochimica Acta Part A: Molecular and Biomolecular Spectroscopy* 324 (2025): 125000.

52. L. Rieppo, S. Saarakkala, T. Närhi, H. J. Helminen, J. S. Jurvelin, and J. Rieppo, "Application of Second Derivative Spectroscopy for Increasing Molecular Specificity of Fourier Transform Infrared Spectroscopic Imaging of Articular Cartilage," *Osteoarthritis and Cartilage* 20 (2012): 451–459.

53. N. P. Camacho, P. West, P. A. Torzilli, and R. Mendelsohn, "FTIR Microscopic Imaging of Collagen and Proteoglycan in Bovine Cartilage," *Biopolymers* 62, no. 1 (2001): 1–8.

54. M. Mehta, R. Naffa, C. Maidment, G. Holmes, and M. Waterland, "Raman and Atr-Ftir Spectroscopy Towards Classification of Wet Blue Bovine Leather Using Ratiometric and Chemometric Analysis," *Journal of Leather Science and Engineering* 2 (2020): 1–15.

55. J. Oinas, L. Rieppo, M. A. J. Finnilä, M. Valkealahti, P. Lehenkari, and S. Saarakkala, "Imaging of Osteoarthritic Human Articular Cartilage Using Fourier Transform Infrared Microspectroscopy Combined With Multivariate and Univariate Analysis," *Scientific Reports* 6 (2016): 1–10.

56. R. Singh, V. Yadav, A. K. Dhillon, A. Sharma, T. Ahuja, and S. Siddhanta, "Emergence of Raman Spectroscopy as a Probing Tool for Theranostics," *Nanotheranostics* 7 (2023): 216–235.

57. P. Casal-Beiroa, V. Balboa-Barreiro, N. Oreiro, S. Pértega-Díaz, F. J. Blanco, and J. Magalhães, "Optical Biomarkers for the Diagnosis of Osteoarthritis Through Raman Spectroscopy: Radiological and Biochemical Validation Using Ex Vivo Human Cartilage Samples," *Diagnostics* 11 (2021): 546.

58. G. Pezzotti, W. Zhu, Y. Terai, et al., "Raman Spectroscopic Insight Into Osteoarthritic Cartilage Regeneration by mRNA Therapeutics Encoding Cartilage-anabolic Transcription Factor Runx1," *Materials Today Bio* 13 (2022): 100210.

59. E. Pavlou, X. Zhang, J. Wang, and N. Kourkoumelis, "Raman Spectroscopy for the Assessment of Osteoarthritis," *Annals of Joint* 3 (2018): 83–83.

60. S. M. Ali, "In Vivo Confocal Raman Spectroscopic Imaging of the human Skin Extracellular Matrix Degradation due to Accumulated Intrinsic and Extrinsic Aging," *Photodermatology, Photoimmunology & Photomedicine* 37 (2021): 140–152.

61. A. Crisford, H. Cook, K. Bourdakos, et al., "Harnessing Raman Spectroscopy and Multimodal Imaging of Cartilage for Osteoarthritis Diagnosis," *Scientific Reports* 14 (2024): 1–17.

62. S. A. Khan, F. N. U. Nidhi, P. C. Amendum, and S. Tomatsu, "Proteoglycans-Methods and Protocols Detection of Glycosaminoglycans in Biological Specimens," *Methods in Molecular Biology (Clifton, NJ)* 2619 (2023): 3.

63. N. Majumder and S. Ghosh, "Unfolding the Mystery Behind the Onset of Chondrocyte Hypertrophy During Chondrogenesis: Toward Designing Advanced Permanent Cartilage-mimetic Biomaterials," *Advanced Functional Materials* 33, no. 35 (2023): 2300651.

64. K. P. Pritzker, S. Gay, S. A. Jimenez, et al., "Osteoarthritis Cartilage Histopathology: Grading and Staging," *Osteoarthritis and Cartilage* 14, no. 1 (2006): 13–29.

65. L. Nagarajan, A. Khatri, A. Sudan, R. Vaishya, and S. Ghosh, "Deep Learning Augmented Osteoarthritis Grading Standardization," *Tissue Engineering Part A* 30, no. 19-20 (2024): 591–604.

66. I. L. Jaabar, P. Cornette, A. Miche, et al., "Deciphering Pathological Remodelling of the Human Cartilage Extracellular Matrix in Osteoarthritis at the Supramolecular Level," *Nanoscale* 14 (2022): 8691–8708.

67. M. Taylor, F. Simoes, J. Smith, et al., "Quantifiable Correlation of ToF-SIMS and XPS Data from Polymer Surfaces with Controlled Amino Acid and Peptide Content," *Surface and Interface Analysis* 54 (2022): 417–432.

68. I. Jaabar, A. Miche, K. Wanherdrick, et al., "Composition and Structure of Human Cartilage Extracellular Matrix: Unravelling Changes During Osteoarthrosis at the Nanoscale," *Osteoarthritis and Cartilage* 29 (2021): S198.

69. E. Pfeiffer, S. M. Vickers, E. Frank, A. J. Grodzinsky, and M. Spector, "The Effects of Glycosaminoglycan Content on the Compressive Modulus of Cartilage Engineered in Type II Collagen Scaffolds," *Osteoarthritis and Cartilage* 16 (2008): 1237–1244.

70. M. Maldonado and J. Nam, "The Role of Changes in Extracellular Matrix of Cartilage in the Presence of Inflammation on the Pathology of Osteoarthritis," *BioMed Research International* 2013 (2013): 284873.

71. X. Bi, X. Yang, M. P. G. Bostrom, and N. P. Camacho, "Fourier Transform Infrared Imaging Spectroscopy Investigations in the Pathogenesis and Repair of Cartilage," *Biochimica Et Biophysica Acta (BBA)—Biomembranes* 1758 (2006): 934–941.

72. Q. Yao, X. Wu, C. Tao, et al., "Osteoarthritis: Pathogenic Signaling Pathways and Therapeutic Targets," *Signal Transduction and Targeted Therapy* 8 (2023): 56.

73. S. Saarakkala and P. Julkunen, "Specificity of Fourier Transform Infrared (FTIR) Microspectroscopy to Estimate Depth-Wise Proteoglycan Content in Normal and Osteoarthritic Human Articular Cartilage," *Cartilage* 1 (2010): 262.

74. L. J. Power, C. Fasolato, A. Barbero, et al., "Sensing Tissue Engineered Cartilage Quality With Raman Spectroscopy and Statistical Learning for the Development of Advanced Characterization Assays," *Biosensors and Bioelectronics* 166 (2020): 112467.

75. Y. Sun, Y. Tsui, M. Yu, et al., "Integration of a Miniaturized DMMB Assay With High-throughput Screening for Identifying Regulators of Proteoglycan Metabolism," *Scientific Reports* 12 (2022): 1083.

76. R. Dreier, "Hypertrophic Differentiation of Chondrocytes in Osteoarthritis: The Developmental Aspect of Degenerative Joint Disorders," *Arthritis Research & Therapy* 12 (2010): 216.

77. P. Gentile, C. Ghione, A. M. Ferreira, A. Crawford, and P. V. Hatton, "Alginate-based Hydrogels Functionalised at the Nanoscale Using Layer-by-layer Assembly for Potential Cartilage Repair," *Biomaterials Science* 5 (2017): 1922–1931.

78. J. Chakraborty, J. Fernández-Pérez, K. A. van Kampen, et al., "Development of a Biomimetic Arch-Like 3D Bioprinted Construct for Cartilage Regeneration Using Gelatin Methacryloyl and Silk Fibroin-gelatin Bioinks," *Biofabrication* 15 (2023): 035009.

79. S. Chawla, G. Desando, E. Gabusi, et al., "The Effect of Silk–gelatin Bioink and TGF-β3 on Mesenchymal Stromal Cells in 3D Bioprinted Chondrogenic Constructs: A Proteomic Study," *Journal of Materials Research* 36 (2021): 4051–4067.

80. C. Roy, M. Roshan, N. Goyal, et al., "MRI Detection and Grading of Knee Osteoarthritis—a Pilot Study Using an AI Technique With a Novel Imaging-based Scoring System," *Biomaterials Science* 13 (2025): 5475–5494.

Supporting Information

Additional supporting information can be found online in the Supporting Information section.

Supporting File: mabi70115-sup-0001-SuppMat.docx.